Chinese Journal of Natural Medicines

Hederagenin attenuates renal senescence in diabetic kidney disease by inhibiting DNMT1–mediated Klotho DNA methylation

Guanfeng Luo, Minyu Liu, Wenbin Yu, Huaxi Liu, Jie Zhou, Dexian Li, Fangxin Chen, Hiu Yee Kwan, Yang Tang, Yanting You, Xiaoshan Zhao, Xiaomin Sun

Citation: Guanfeng Luo, Minyu Liu, Wenbin Yu, Huaxi Liu, Jie Zhou, Dexian Li, Fangxin Chen, Hiu Yee Kwan, Yang Tang, Yanting You, Xiaoshan Zhao, Xiaomin Sun, Hederagenin attenuates renal senescence in diabetic kidney disease by inhibiting DNMT1–mediated Klotho DNA methylation, Chinese Journal of Natural Medicines, 2026, 24(9), 1094–1109. doi: 10.1016/S1875–5364(26)61205–8.

View online: https://doi.org/10.1016/S1875–5364(26)61205–8

Related articles that may interest you

Dihydroartemisinin attenuates ischemia/reperfusion–induced renal tubular senescence by activating autophagy

Chinese Journal of Natural Medicines. 2023, 21(9), 682–693 https://doi.org/10.1016/S1875–5364(23)60398–X

Bear bile powder alleviates Parkinson's disease–like behavior in mice by inhibiting astrocyte–mediated neuroinflammation

Chinese Journal of Natural Medicines. 2023, 21(9), 710–720 https://doi.org/10.1016/S1875–5364(23)60449–2

Metabolomics analysis reveals the renal protective effect of *Panax ginseng* C. A. Mey in type 1 diabetic rats

Chinese Journal of Natural Medicines. 2022, 20(5), 378–386 https://doi.org/10.1016/S1875–5364(22)60175–4

Lignans with (*N*, *N*–diethyl)methyl amino group from *Buxus rugulosa*

Chinese Journal of Natural Medicines. 2021, 19(9), 675–679 https://doi.org/10.1016/S1875–5364(21)60064–X

Eucommia lignans alleviate the progression of diabetic nephropathy through mediating the AR/Nrf2/HO–1/AMPK axis *in vivo* and *in vitro*

Chinese Journal of Natural Medicines. 2023, 21(7), 516–526 https://doi.org/10.1016/S1875–5364(23)60427–3

Shen Qi Wan attenuates renal interstitial fibrosis through upregulating AQP1

Chinese Journal of Natural Medicines. 2023, 21(5), 359–370 https://doi.org/10.1016/S1875–5364(23)60453–4

Wechat

Chinese Journal of Natural Medicines 24 (2026) 1094-1109

Contents lists available at ScienceDirect

Chinese Journal of Natural Medicines

journal homepage: www.cjnmcpu.com/

Original article

Hederagenin attenuates renal senescence in diabetic kidney disease by inhibiting DNMT1-mediated Klotho DNA methylation

Guanfeng Luo[a, e,Δ], Minyu Liu[a,Δ], Wenbin Yu[a,Δ], Huaxi Liu[c], Jie Zhou[a], Dexian Li[a], Fangxin Chen[a], Hiu Yee Kwan[d], Yang Tang[f], Yanting You[a,*], Xiaoshan Zhao[a,*], Xiaomin Sun[a, b, e,*]

[a] *School of Traditional Chinese Medicine, Southern Medical University, Guangzhou 510515, China*
[b] *Southern Medical University Hospital of Integrated Traditional Chinese and Western Medicine, Southern Medical University, Guangzhou 510315, China*
[c] *Boai Hospital of Zhongshan, Zhongshan 528403, China*
[d] *School of Chinese Medicine, Hong Kong Baptist University, Hong Kong, China*
[e] *Guangdong Basic Research Center of Excellence for Integrated Traditional and Western Medicine for Qingzhi Diseases, Guangzhou 510515, China*
[f] *Department of Traditional Chinese Medicine, The First Affiliated Hospital of Gannan Medical University, Ganzhou 341000, China*

ARTICLE INFO

Article history:
Received 26 February 2026
Revised 24 May 2026
Accepted 26 May 2026
Available online 20 September 2026

Keywords:
Diabetic kidney disease
Hederagenin
DNA methylation
Senescence
Klotho

ABSTRACT

Background Hederagenin is a naturally occurring pentacyclic triterpenoid found in several medicinal plants traditionally used for treating renal and metabolic disorders. Its ability to mitigate renal senescence in diabetic kidney disease (DKD) and the associated epigenetic mechanisms have not yet been fully elucidated. Methods db/db mice were used *in vivo* to model DKD-associated renal senescence, while palmitic acid-treated human renal proximal tubular epithelial cells (HK-2 cells) were used *in vitro* as a senescence model. Renal injury, senescence, DNA damage, and Klotho expression were evaluated using histological, biochemical, and molecular analyses. GEO datasets derived from human DKD samples and corresponding controls were analyzed to assess Klotho expression. Integrated target-binding and methylation analyses were performed to examine the interaction between hederagenin and DNA methyltransferase 1 (DNMT1), as well as the effects of hederagenin on Klotho promoter methylation and DNMT1 occupancy. Results Hederagenin reduced renal senescence, fibrosis, and DNA damage *in vivo* and *in vitro*, while restoring Klotho expression, which was decreased in patient datasets and experimental models. Mechanistically, hederagenin directly bound DNMT1, diminished DNMT1 recruitment to the Klotho promoter, and attenuated aberrant promoter hypermethylation, thereby reactivating Klotho. Conclusion Hederagenin mitigates renal senescence in DKD through a DNMT1–Klotho DNA methylation axis, supporting its ethnopharmacological potential for DKD management.

1. Introduction

Diabetic kidney disease (DKD), arising from diabetes-related kidney injury, constitutes the primary contributor to chronic kidney disease (CKD). An imbalance in glucose metabolism is the root cause of DKD, which in turn accelerates the disease's progression through metabolic, hemodynamic, inflammatory, and fibrotic mechanisms. [1] In recent years, several new therapies for DKD have emerged, such as sodium-glucose cotransporter 2 inhibitors and drugs targeting the renin-angiotensin-aldosterone system [2, 3]. Unfortunately, for the majority of people with DKD, these treatments do not entirely reverse the disease's effects on renal function. Therefore, new therapeutic approaches are urgently required. Renal fibrosis is increasingly recognized as a final common pathway driving chronic progression of DKD, and emerging nanotechnology-enabled strategies are providing new opportunities for antifibrotic intervention [4].

Hederagenin (Hed), a pentacyclic triterpenoid found in nature, is obtained from various medicinal plants such as *Hedera nepalensis* var. *sinensis* (Tobl.) Rehd, *Astragalus membranaceus* (Fisch.) Bunge and Paeoniae Radix Alba. Hed and its derivatives, a triterpenoid constituent occurring in these medicinal materials, exhibit multiple pharmacological activities, including anti-inflammatory, metabolic, antifibrotic, renoprotective effects [5]. There is some evidence that Hed could be used medicinally to treat kidney problems, both chronic and acute [6-8]. In particular, Hed reduces ferroptosis-induced renal fibrosis in DKD *via* inhibiting Smad3 phosphorylation, which in turn decreases NOX4 expression and increases GPX4 expression [9]. High glucose-induced renal cell fibrosis is reduced by Hed *via* the downregulation of CTSB expression, which subsequently blocks NLRP3 inflammasome activation [10]. Collectively, these findings support Hed as an ethnopharmacology-informed candidate for targeting DKD. In line with this, recent bibliometric analyses have highlighted the growing research interest in natural products as multi-target therapeutic agents for DKD [11]. However, despite this increasing attention, the therapeutic effects of Hed and its underlying mechanisms in

* Corresponding author.
E-mail addresses: 602704314@qq.com (Y. You); zhaoxs0609@163.com (X. Zhao); min1980@smu.edu.cn (X. Sun)
Δ These authors contributed equally to this work.

https://doi.org/10.1016/S1875-5364(26)61205-8
Copyright © 2026, China Pharmaceutical University. Published by Elsevier B.V. All rights are reserved.

DKD—particularly those related to cellular senescence and epigenetic regulation—remain to be fully elucidated.

DNA methylation primarily suppresses transcription by interfering with transcription factors' ability to attach to their specific DNA elements. This modification serves as a durable and transmissible epigenetic mark within eukaryotic cells [12]. Among the many epigenetic abnormalities seen in DKD communities around the world, aberrant DNA methylation stands out. In addition to other risk factors, these DNA methylation abnormalities advance DKD, especially in genes implicated in important metabolic pathways. DNA methylation alterations in genes that function within pathogenic pathways, particularly those linked to fibrosis and inflammation, are considered important molecular markers in DKD progression [13]. However, the mechanisms by which DNA methyltransferase 1 (DNMT1), a key DNA methylation enzyme, regulates aging in DKD remain incompletely understood. Moreover, as shown by multiple clinical trials, its diagnostic or prognostic efficacy is still inadequate. Therefore, there is an urgent need for deeper exploration of how DNA methylation contributes to renal senescence. Current research indicates that inhibiting the increase in DNA methyltransferase can restore antioxidant anti-aging inhibitors and improve renal aging [14].

Klotho is an important gene in the ageing process of mammals that has been discovered over the years. Research on DKD has demonstrated that Klotho can delay the aging process and preserve cells from harm [14, 15]. Furthermore, Klotho expression varies with both the duration and severity of diabetes, implying that it could function as an early biomarker for DKD [16, 17]. Consequently, adjusting Klotho activity emerges as a potential therapeutic avenue for aging-related diseases, with particular relevance to DKD marked by Klotho dysregulation.

Thus, we investigated how Hed regulates Klotho DNA methylation in DKD. It was found that DNMT1 interacts with Hed, resulting in a reduction of DNA methylation at the Klotho gene. As a consequence, Klotho is upregulated, resulting in diminished DNA damage and a retardation of renal aging in DKD.

2. Materials and methods

2.1. Reagents

HPLC analysis confirmed that Hed, supplied by Sichuan Weikeqi Biological Technology Co., Ltd., has a purity of over 98%.

2.2. Cells culture and treatment

HK-2 cells (Procell Life Science & Technology, Wuhan, China) were cultured in MEM medium (Biolnd, Israel) supplemented with 10% fetal bovine serum (Biolnd) and 1% penicillin-streptomycin. The cells were maintained at 37 °C with 5% CO_2 under humidified conditions. Cells were sub-cultured every 2 days, and passages 3–10 were applied for experimental procedures. HK-2 cells were exposed to palmitic acid (PA; 400 μmol·L^{-1}, Sigma-Aldrich, USA) for 48 h to induce senescence. For intervention experiments, cells were co-treated with PA and hederagenin (Hed; 12.5, 25, or 50 μmol·L^{-1}) for 48 h. Where indicated, 5-azacitidine (5-AZA; 50 μmol·L^{-1}, InvivoChem, Guangzhou, China) was used as a positive control and co-incubated with PA for 48 h. The normal control consisted of untreated HK-2 cells, while HK-2 cells treated with 400 μmol·L^{-1} PA were designated as the senescence model.

2.3. Animals and treatment

Male C57BLKs/J db/m and db/db mice, aged six weeks, were purchased from Changzhou Cavens Model Animal Co., Ltd. and housed in a specific pathogen-free (SPF) facility at 22 ± 2 °C, 50%–60% relative humidity, with a 12-hour light/dark photoperiod. Six groups were formed by random allocation of the mice: control (db/m, n = 7), model (db/db, n = 7), Hed-L (2.5 mg·kg^{-1} hederagenin, n = 7), Hed-M (5 mg·kg^{-1} hederagenin, n = 7), Hed-H (10 mg·kg^{-1} hederagenin, n = 7), and dapagliflozin (1 mg·kg^{-1}, n = 7). The normal control group consisted of db/m mice, whereas db/db mice were designated as the DKD model. Daily gavage with 0.1% DMSO (using 0.5% CMC-Na as the diluent) was initiated at 8 weeks of age for db/db mice in the control and model groups. Concurrently, mice in the Hed and dapagliflozin groups were orally administered their respective drugs *via* gavage for 12 consecutive weeks. Both dapagliflozin and Hed were initially dissolved in DMSO and then diluted using 0.5% CMC-Na. Ultimately, the final solution contained 0.1% DMSO. The doses of hederagenin (2.5, 5, and 10 mg·kg^{-1}) were selected with reference to previous mouse studies showing renoprotective effects of hederagenin in kidney disease models, in which effective oral doses ranged from 20 to 40 mg·kg^{-1}·d^{-1} [5]. Considering the prolonged 12-week administration in db/db mice, a lower low-/medium-/high-dose regimen was adopted in the present study to evaluate dose-dependent efficacy while maintaining an acceptable safety margin. Blood glucose levels were checked every two weeks. To obtain 24-hour urine samples after 12 weeks of treatment, each mouse was housed in an individual metabolic cage. Euthanasia was subsequently carried out at week 20 *via* intraperitoneal injection of pentobarbital sodium at a dose of 50 mg·kg^{-1}. Serum samples and kidney tissues were isolated and prepared for additional experiments. Double-blinded principles were employed throughout the animal procedures. Prior to the initiation of experiments, all animal procedures received ethical approval from the Animal Ethics Committee of Southern Medical University (Approval No. SMUL202410018) and were also reviewed and approved by the China Council on Animal Care and Use.

2.4. Histological analysis, immunohistochemistry (IHC) and SA-β-galactosidase Staining

Sections measuring 4 μm thick were cut from the kidney tissues that had been treated with formalin and then embedded in paraffin. The histological alterations in the kidneys were examined by staining the sections with H&E and Masson. For immunohistochemistry, sections were heated in Tris-EDTA buffer (pH 9.0) at 98 °C for 10 min. Primary antibodies included γ-H2AX (1∶500, Proteintech, Wuhan, China) and Klotho (1∶200, Proteintech, Wuhan, China). Stained sections were examined under an optical microscope, and ImageJ was applied to quantify positive γ-H2AX and Klotho signals. SA-β-galactosidase staining was conducted using a commercial kit (C0602, Beyotime, China) following the instructions supplied by the manufacturer.

2.5. Biochemical measurements

After collection from the abdominal aorta, blood samples were centrifuged at 3500 r·min^{-1} for 10 min. Serum creatinine (Scr) and blood urea nitrogen (BUN) were determined using the Creatinine Assay kit (C011-2-1) and Urea Assay kit (C013-1-1) obtained from Nanjing Jiancheng Bioengineering Institute (Nanjing, China). The 24-hour urinary total protein (24 h UTP) was measured with a urine protein assay kit (C035-2-1, Nanjing Jiancheng Bioengineering Institute, Nanjing, China).

2.6. Cell viability

The CCK-8 assay was employed to assess the viability of HK-2 cells. Cells were seeded in 96-well plates at a density of 6000 cells per well and treated following the experimental design. Follow-

ing treatment, 10 μL of CCK-8 reagent (#521942, Bioshark, Hefei, China) was introduced into each well, and the plates were incubated at standard culture conditions for 30 min. We measured the absorbance at 450 nm.

2.7. Immunofluorescence

Immunofluorescence assays were conducted by seeding 2 × 10^5 cells per well on coverslips in 6-well plates. Cells were subjected to three PBS washes before being fixed in 4% paraformaldehyde. Subsequently, the cells were incubated in PBS containing 5% bovine serum albumin for 1 h to block non-specific binding. Primary antibodies were applied to the samples and left to incubate overnight at 4 °C. Following three consecutive PBS washes of 15 min each, secondary antibodies were added to the cells and incubated at ambient temperature for 1 h. Cells were then stained with 5 μg·mL^{-1} Hoechst 33342 for 20 min. Visualization was carried out using a Leica inverted fluorescence microscope (LEICA DMi8), with image coloring and merging conducted in Leica Application Suite X.

The kFluor488 Click-iT EdU Imaging Kit (KGA9602, Keygen, Nanjing, China) was used to determine cell proliferation in line with the manufacturer's guidelines. EdU (20 μmol·L^{-1}) was incorporated into the culture medium for 2 h. Cells were first fixed and permeabilized. They were then incubated with the Click-iT reaction cocktail for 30 min and counterstained with 5 μg·mL^{-1} Hoechst 33342 for 20 min. Samples were kept protected from light, and images were acquired and processed on a Leica inverted fluorescence microscope.

2.8. The cell cycle

Using a Cell Cycle Detection Kit (KGA9101, Keygen, Nanjing, China), the cell cycle of treated cells was determined as per the manufacturer's protocol. Cells underwent fixation in 70% ethanol overnight. They were subsequently stained with RNase and PI for 30 min. Samples were analyzed by flow cytometry using a CytoFLEX S instrument (Beckman Coulter, USA). FlowJo software was then used to evaluate the results.

2.9. Western blot (WB)

Kidney tissues and cultured cells underwent lysis in RIPA buffer. Total protein levels were subsequently determined using a BCA Protein Assay Kit (P0011, Beyotime, Shanghai, China). Proteins of equal amounts were loaded onto 12%–15% SDS-PAGE gels for separation and subsequently transferred to PVDF membranes. Membranes underwent blocking with 5% non-fat milk for 2 h. They were subsequently incubated overnight at 4 °C with the indicated primary antibodies: anti-N-cadherin (1∶1000, Cell Signaling Technology, USA), anti-Klotho (1∶1000, Proteintech, Wuhan, China), anti-Vimentin (1∶1000, Proteintech, Wuhan, China), anti-P53 (1∶1000, Proteintech, Wuhan, China), anti-α-SMA (1∶1000, Proteintech, Wuhan, China), anti-P21 (1∶500, Proteintech, Wuhan, China), anti-P16 (1∶2000, Proteintech, Wuhan, China), and anti-β-actin (1∶3000, Affinity, USA). Secondary antibodies (1∶3000, Cell Signaling Technology, USA) were applied for 1 h at room temperature. Chemiluminescent detection was performed using the ECL system. Band intensities were subsequently measured with Image*J* software.

2.10. Data acquisition and computational analysis

Datasets GSE30529, GSE96804, and GSE142025 were retrieved from the Gene Expression Omnibus (GEO) database(https://www.ncbi.nlm.nih.gov/geo/) to identify differentially expressed genes between normal and DKD kidney samples. GSE30529 contains transcriptomic data from human renal tubulointerstitial/tubular samples, including 10 DKD samples and 12 control samples. GSE96804 contains glomerular transcriptomic profiles from 41 DKD samples and 20 normal control samples. GSE142025 contains RNA-seq data from whole-kidney biopsy samples, including 28 biopsy-proven DN samples (6 early DN and 22 advanced DN) and 9 normal nephrectomy control samples. Expression data were analyzed using a standard limma workflow in R, with routine preprocessing and normalization performed prior to differential expression analysis. Differentially expressed genes were identified using the criteria of adjusted $P < 0.05$ and $|\log_2 FC| > 1$. Gene Set Enrichment Analysis (GSEA) was conducted using GSEA version 3.10.1 (https://www.omicstudio.cn/tool/29).

2.11. DNMT1 overexpression and DNMT1/Klotho gene silencing via transfection

Transfection was performed on HK-2 cells seeded in 12-well plates when cell confluence reached 40%–60%. Cells were treated with siRNAs specific for Klotho or DNMT1, a DNMT1 overexpression plasmid, or their respective negative controls using Lipofectamine 6000 (Beyotime, Shanghai, China). The siRNAs and overexpression plasmids targeting Klotho and DNMT1, as well as corresponding negative controls, were custom-prepared by RiboBio Co., Ltd. (Guangzhou, China).

2.12. Molecular docking

To explore the interaction between Hed and DNMT1, molecular docking was performed. Three-dimensional structures of Hed and DNMT1 were retrieved from PubChem (CID: 73299) and the Protein Data Bank (PDB ID: 3SWR), respectively. Binding site analysis and visualization were carried out using Discovery Studio (Accelrys, San Diego, USA), and binding affinity was evaluated with AutoDockTools 1.5.6.

2.13. Molecular dynamics (MD) simulation

In brief, following the literature protocol [18], the optimal docking conformation served as the initial structure for molecular dynamics (MD) simulations performed using YASARA. Molecular dynamics calculations were performed using the AMBER 03 force field. The DNMT1–Hed complex was solvated in a saline dodecahedral box with a minimum distance of 5 Å between the solute and the box edge. Simulated annealing minimization was initiated at 298 K, with velocities scaled by 0.9 every 10 steps for a total of 5 ps. After energy minimization, temperature regulation and thermal stabilization were achieved using the Berendsen thermostat. The production run lasted 100 ns with a 2 fs time step, and structural coordinates were saved every 10 ps.

2.14. Surface plasmon resonance

Surface plasmon resonance (SPR) was applied using the PlexArray® HT System (Plexera, Guangzhou, China) to investigate Hed–DNMT1 interactions, allowing real-time monitoring throughout the experiment. DNMT1 protein (1 mg·mL^{-1}; BIOESN, Shanghai, China) was coupled to a 3D dextran sensor chip (Plexera, Beijing, China) using a conventional amine coupling strategy with 0.4 mol·L^{-1} EDC and 0.1 mol·L^{-1} NHS. Hed was diluted in PBS to final concentrations of 10, 20, 30, 40, and 50 μmol·L^{-1}, while chip regeneration was achieved using 10 mmol·L^{-1} glycine–HCl (pH 2.0). SPR measurements were performed at 22 °C with a flow rate of 2 μL·s^{-1}, and both the association and dissociation phases were maintained for 300 s. Binding interactions and kinetic parameters were analyzed based on SPR response changes using the

BIA evaluation software (GE Healthcare).

2.15. Cellular thermal shift assay (CETSA) and drug affinity responsive target stability (DARTS)

The association of Hed with DNMT1 was assessed using CETSA and DARTS assays. Shaking was used for three h at 4 °C to treat HK-2 cell lysate with either DMSO or Hed (50 μmol·L^{-1}) for CETSA. The substance was thereafter divided into individual tubes and subjected to varying degrees of heat for a duration of 3 min. The lysate was first cooled and centrifuged at 12 000 r·min^{-1} for 15 min at 4 °C. The clarified supernatant was subsequently isolated for Western blot analysis.

For DARTS, the HK-2 cell lysate was aliquoted into individual tubes and subjected to incubation at 4 °C for 3 h with either DMSO or Hed. Subsequently, the samples were treated with varying concentrations of Pronase E (Roche, Switzerland) and maintained at ambient temperature for 10 min. Untreated lysates served as controls. The materials were heated for Western blot analysis after adding a loading buffer to halt the processes.

2.16. Methylation-specific PCR (MSP) and bisulfite sequencing PCR(BSP)

A universal genomic DNA extraction kit called SteadyPure (AG21009, Changsha, China) was used to extract the DNA. The DNA samples were bisulfite-converted using the DNA Bisulfite Conversion Kit (DP215, TIANGEN, Beijing, China) following extraction. The bisulfite-converted genomic DNA was subsequently subjected to polymerase chain reaction (PCR) using methylation-specific primers from Invitrogen and the MethyTect Taq HS PCR kit for bisulfite-treated DNA (AG11209, Changsha, China). Electrophoresis was used to examine the MSP products on a Biosharp 3% agarose gel located in Hefei, China.

For BSP, genomic DNA was extracted from the samples using a high-efficiency kit according to the manufacturer's instructions, ensuring a cell count greater than 10^6 and DNA concentrations of 200–600 ng·μL^{-1} with an OD_{260}/OD_{280} ratio between 1.8 and 2.0. The DNA was subsequently bisulfite-converted using a DNA Bisulfite Conversion Kit by combining it with buffer DP and Bisulfite Mix, then subjecting it to thermal cycling at 95 °C for 10 min, 64 °C for 30–60 min, and finally maintaining at 4 °C. The bisulfite-converted DNA was cleaned using spin columns. PCR amplification was performed with bisulfite-specific primers targeting the human Klotho (hKL) promoter region (hKL-BSP-F and hKL-BSP-R; Supplementary Table S1). The BSP amplicon was 160 bp in length and encompassed 15 CpG sites (CpG1–CpG15), which were numbered from 5' to 3' according to their positions within the amplified region. PCR products were cloned into a vector and transformed into *E. coli*. After colony selection, at least 10 independent clones per sample were subjected to Sanger sequencing. Bisulfite conversion efficiency was verified by confirming near-complete conversion of non-CpG cytosines to thymine in the sequencing reads. Methylation levels of the target region were determined from sequencing results by scoring methylated versus unmethylated CpG sites across CpG1–CpG15.

2.17. Chromatin immunoprecipitation-quantitative polymerase chain reaction (ChIP-qPCR)

ChIP was executed using the SimpleChIP® Enzymatic Chromatin IP Kit (9003, Cell Signaling Technology, USA), adhering to the manufacturer-provided protocol. Briefly, cells were collected in 10-cm culture dishes at a density of 4 × 10^6, followed by cross-linking and chromatin fragmentation by sonication. Immunoprecipitation of the sheared chromatin was then carried out using an anti-DNMT1 antibody (5032, Cell Signaling Technology, USA). Proteinase K was employed to degrade proteins, and sodium chloride was applied to reverse cross-links. The enriched DNA fragments were subjected to phenol/chloroform extraction and ethanol precipitation to obtain purified DNA. Following purification, DNA was assessed by real-time quantitative PCR using primers targeting the predicted BSP site in the Klotho gene (Supplementary Table S1).

2.18. Electrophoretic mobility shift assay (EMSA)

EMSA was conducted to examine the binding between DNMT1 and the Klotho promoter DNA fragment. A double-stranded DNA probe corresponding to the CpG-rich region of the human Klotho promoter was synthesized, with the 5'-biotin-labeled sense strand. Probe sequence: 5'-Biotin-GCGGCGCGCTCCGCTAGGGCCCGGCAGGATCCCGCCCCCAAGTCGGGG-3'. Equimolar oligonucleotides (sense and complementary antisense strands) were annealed by heating at 95 °C for 5 min followed by gradual cooling to room temperature.

Binding reactions were conducted using a commercial EMSA kit (Thermo Fisher Scientific, 20158) following the manufacturer's instructions. Briefly, purified recombinant target protein was incubated with the biotin-labeled DNA probe in binding buffer at room temperature for 20 min. For drug treatment groups, Hed (50 μmol·L^{-1}) and 5-AZA (50 μmol·L^{-1}) were added to the reaction mixture prior to probe addition. Control reactions included probe alone or probe incubated with DNMT1 without Hed and 5-AZA. DNA-protein complexes were resolved on a non-denaturing 6% polyacrylamide gel in 0.5 × TBE buffer, electrophoresed at 100 V for about 70 min at 4 °C Post-electrophoresis, complexes were transferred to a nylon membrane and cross-linked by ultraviolet irradiation. Biotin-labeled DNA was detected with streptavidin-horseradish peroxidase conjugate and visualized by chemiluminescence.

2.19. DNA pull down

Biotin-labeled DNA fragments derived from the human Klotho promoter were amplified by PCR using a 5'-biotin-modified forward primer (h-PD-F) and an unlabeled reverse primer (h-PD-R), followed by agarose gel purification and quantification. Streptavidin magnetic beads were subjected to three washes with binding buffer (50 mmol·L^{-1} Tris-HCl, pH 7.5; 150 mmol·L^{-1} NaCl; 1 mmol·L^{-1} EDTA; 0.05% NP-40; 10% glycerol; containing protease inhibitors). They were then ready for subsequent use. Then, 5 μg biotin-labeled DNA was incubated with streptavidin beads at ambient temperature for 30 min with gentle rotation to generate DNA-bead complexes. After washing, the complexes were incubated with purified DNMT1 protein in binding buffer at 4 °C for 2–4 h; for drug treatment groups, Hed and 5-AZA added during incubation. The beads underwent sequential washes with low-salt (150 mmol·L^{-1} NaCl) and medium-salt (300 mmol·L^{-1} NaCl) buffers, followed by a detergent-free wash to minimize non-specific binding. Bound proteins were eluted by boiling in 2 × SDS loading buffer for 5 min, and analyzed by SDS-PAGE and immunoblotting. Input samples and negative controls (beads-only) were included in parallel.

2.20. Statistical analysis

SPSS 26.0 was used for statistical analysis, and GraphPad Prism 8.0 for figure generation. Values are expressed as mean ± SD. An independent samples t-test compared two groups, and one-way ANOVA assessed differences among multiple groups. When variances were equal, the Least Significant Difference test was employed; otherwise, Dunnett's T3 test was applied. Statistical significance was defined as $P < 0.05$.

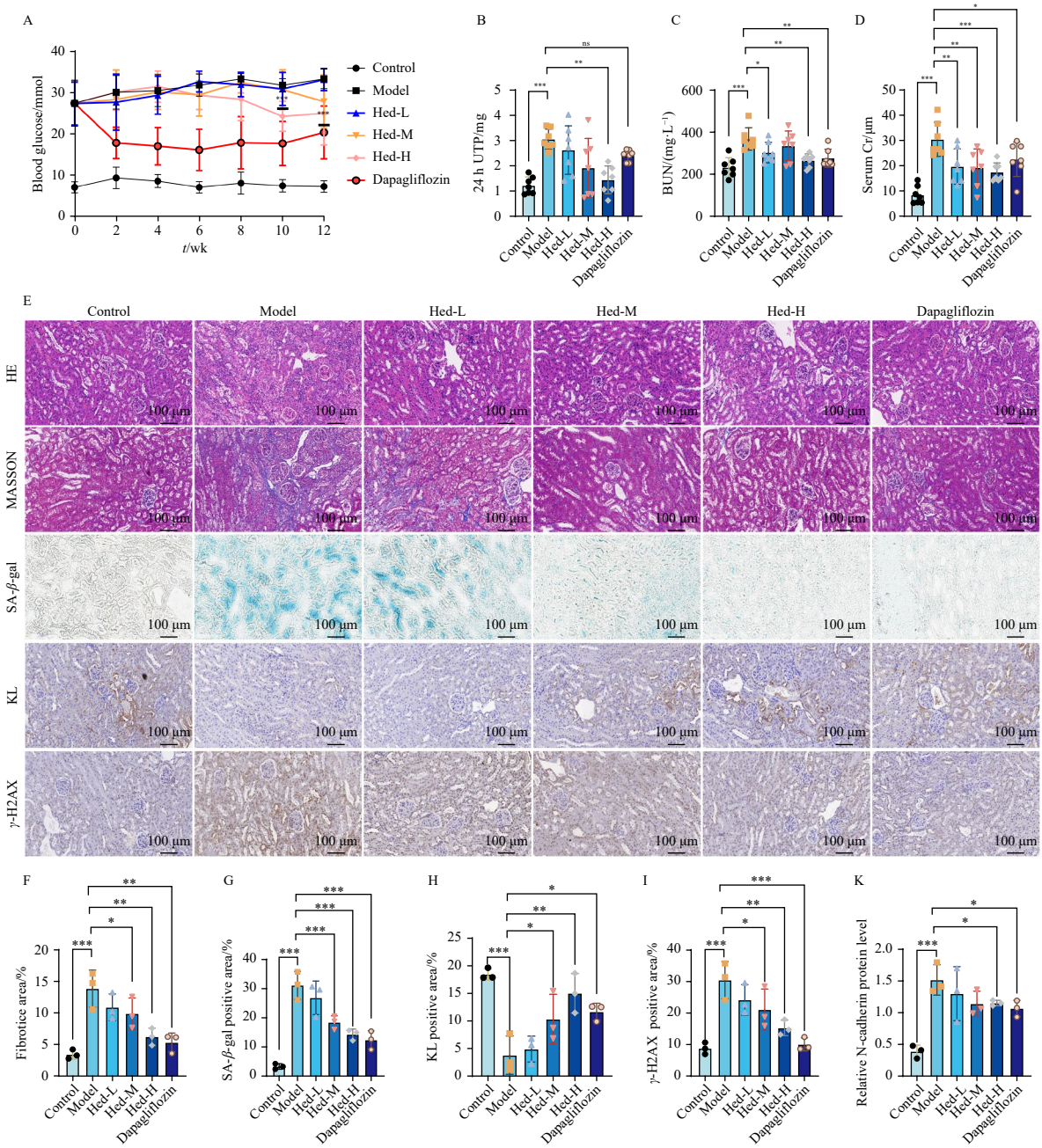
3. Results

3.1. Hed improves renal senescence and pathological damage in db/db mice

To assess Hed's therapeutic impact on renal function in DKD, db/db mice received different doses of Hed. Hed treatment markedly decreased serum BUN levels in db/db mice. Furthermore, high-dose Hed (10 mg·kg^{-1}) administration markedly reduced blood glucose levels during the later stages of treatment (weeks 10–12). While this effect was notable, it occurred later compared to the early glucose-lowering effect observed with the reference drug Dapagliflozin (1 mg·kg^{-1}). Notably, Hed exerted a more pronounced effect on 24-hour urinary total protein (24 h UTP) and serum creatinine (Scr) levels than dapagliflozin (Figs. 1A–1D). Histopathological evaluation provides direct evidence of renal structural injury. H&E staining revealed severe damage to renal tubular epithelial cells in DKD mice, characterized by tubular dilation, deformation, and extensive inflammatory cell infiltration within the interstitium. Consistently, Masson's trichrome staining indicated markedly increased fibrotic accumulation in the kidneys of db/db mice. SA-β-galactosidase staining further revealed increased renal cellular senescence. Hed treatment significantly improved renal function and mitigated histopathological injury in db/db mice. Immunohistochemical analysis of Klotho and γ-H2AX, markers associated with senescence and DNA damage, further supported the renoprotective role of Hed. Hed administration effectively reversed γ-H2AX upregulation and restored Klotho expression (Figs. 1E–1I). Western blot analysis of senescence- and fibrosis-associated proteins—including Klotho, P53, P21, P16, N-cadherin, Vimentin, and α-SMA—provided additional confirmation of these results. Figs. 1J–1Q reveal that Hed restored Klotho levels and considerably decreased senescence and fibrosis markers in kidney tissue.

3.2. Hed attenuates PA-induced senescence in HK-2 cells

Cells were treated with PA for 48 h in order to evaluate its role in promoting stress-induced senescence in HK-2 cells. EdU



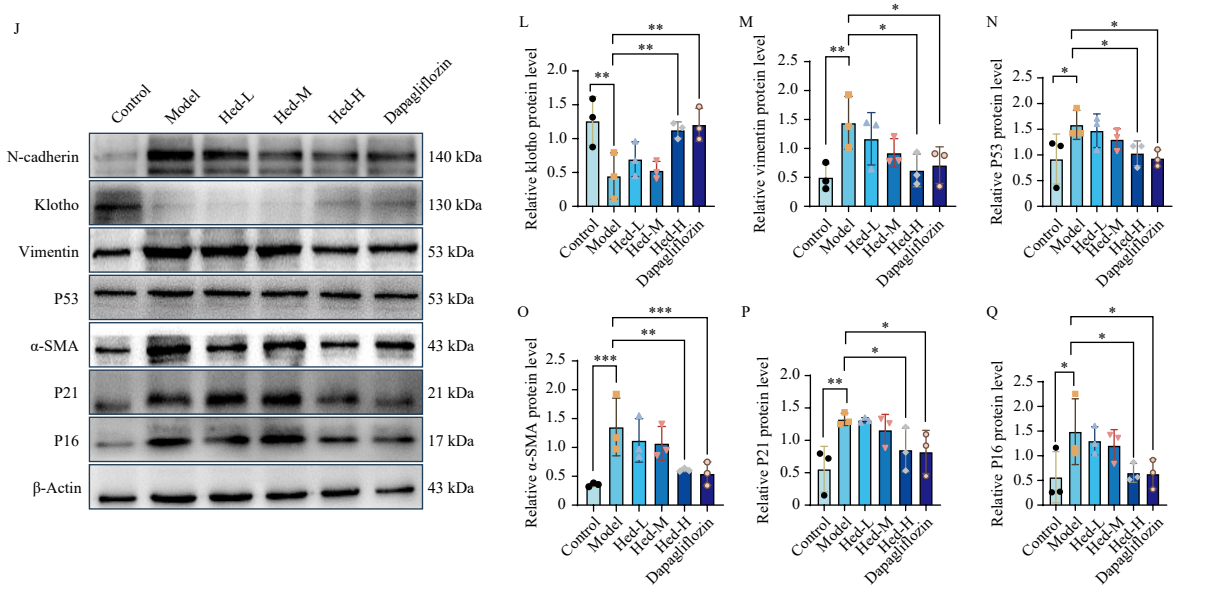


Fig. 1 Hed protects against renal senescence and pathological damage in db/db mice. (A) Blood glucose levels. (B) 24-hour urine total protein. (C, D) The BUN and Scr levels (n = 7 mice per group). (E–I) H&E, Masson and senescence-associated β-galactosidase staining of kidney sections, IHC sections and quantitative results of renal fibrosis and β-galactosidase, Klotho and γ-H2AX staining. (J–Q) Western blot analysis and quantitative results of N-cadherin, Klotho, Vimentin, P53, α-SMA, P21 and P16 (n = 3 each, experiments performed in triplicate). Data are mean ± SD. Statistical analysis was performed using one-way ANOVA followed by LSD post hoc test. $^{*}P < 0.05$, $^{**}P < 0.01$, $^{***}P < 0.001$, NS, not significant. All microscopic images were captured at × 20 magnification. Scale bar = 100 μm.

incorporation was reduced in response to escalating PA concentrations, as demonstrated by EDU staining (Figs. S1a and S1g). CCK-8 assays indicated that cell proliferation declined significantly at higher PA concentrations (Fig. S1h). Figs. S1d and S1r demonstrated that PA treatment altered cell cycle distribution in HK-2 cells, accompanied by a reduction in the G_2/M population, consistent with impaired cell cycle progression. Together with increased SA-β-gal staining (Figs. S1b and S1j), these results suggest that PA induces a senescence-associated growth arrest in HK-2 cells. Proteins associated with senescence and fibrosis were upregulated in response to PA treatments, while proteins involved with Klotho were downregulated (Figs. S1f, S1k, and S1q). Increasing concentrations of PA led to elevated γ-H2AX levels, indicating DNA damage, as shown in Figs. S1c and S1i. HK-2 cells treated with PA exhibited increased senescence and fibrosis. Among the tested concentrations, 400 μmol·L^{-1} produced the most significant responses. In addition, Annexin V/PI staining showed no marked increase in apoptotic cells following PA treatment (Fig. S1e), indicating that PA-induced growth arrest was not primarily attributable to apoptosis. Preliminary optimization indicated that 400 μmol·L^{-1} PA most effectively induced senescence. This concentration was applied in the subsequent experiments.

To examine how Hed affects PA-induced senescence, HK-2 cells were simultaneously exposed to 400 μmol·L^{-1} PA and 12.5, 25, or 50 μmol·L^{-1} Hed for 48 h. Hed promoted cell proliferation again, as seen in Figs. 2A, 2F, and 2G. Simultaneously, Hed also restored the G_2/M cell number (Figs. 2D and 2J). Figs. 2B and 2H demonstrated that exposure to PA induced a pronounced rise in SA-β-gal-positive cells. Administration of Hed mitigated this effect, showing a clear dose-dependent reduction. Also, in a dose-dependent fashion, the addition of Hed suppressed the PA-induced upregulation of P16, P21, and P53 protein expression. Similarly, Figs. 2E and 2K–2Q indicated that Hed treatment during PA exposure restored Klotho protein levels and concurrently decreased levels of fibrosis-related proteins. PA exposure increased γ-H2AX in cells (Figs. 2C and 2I), while Hed treatment reduced DNA damage in a manner dependent on the administered dose. In general, the fibrosis and senescence of HK-2 cells caused by PA therapy were partially alleviated by Hed addition.

3.3. Reduced Klotho in DKD patients may be linked to the acceleration of renal senescence.

To identify genes contributing to renal senescence in DKD, we analyzed the GEO database and initially screened 190 differentially expressed genes (Figs. 3A–3D). Using an expression cutoff, 31 genes were selected (Figs. 3E–3F) and found to correlate with renal senescence based on GSEA results (Fig. 3G). Klotho levels were notably lower in DKD patients (Figs. 3H–3J), highlighting its key regulatory function in renal senescence linked to DKD.

3.4. Klotho is essential for Hed-mediated suppression of senescence.

We transfected cells with si-Klotho to knock down Klotho expression, which allowed us to delve deeper into how Hed controls renal senescence in DKD. Figs. 4A, 4B, and 4F–4H showed that HK-2 cell proliferation was markedly decreased, with a corresponding rise in SA-β-gal-positive cells. Figs. 4C, 4D, 4I, and 4J show a reduction in the G_2 phase cell fraction, along with elevated γ-H2AX expression. Following Klotho knockdown, Hed treatment did not restore Klotho expression (Figs. 4E and 4K). Similarly, it failed to mitigate senescence in HK-2 cells. In summary, silencing the Klotho gene eliminates Hed's protective impact against cellular senescence, suggesting that Hed mitigates renal aging in DKD primarily through controlling Klotho levels.

An epigenetic mechanism regulates Klotho expression, according to previous research [14]. Hypermethylated CpGs typically occur in repressed or lowly expressed genes, while hypomethylated CpGs are found in actively and constitutively expressed promoter regions [19]. To examine possible involvement of abnormal DNA methylation in Klotho downregulation, human Klotho gene promoters were analyzed using MethPrimer (http://www.urogene.org/methprimer) (Fig. S2). Subsequently, we assessed DNA methylation at the Klotho promoter in HK-2 cells following PA treatment and found a significant increase from 44.52% ± 1.80% to 61.53% ± 4.48% compared with untreated cells ($P < 0.01$). As shown in Figs. 4L–4M, co-treatment with Hed reduced DNA methylation at the Klotho promoter from 61.53% ± 4.48% in PA-treated HK-2 cells to 56.17% ± 5.11% ($P < 0.05$). Similar results were obtained using BSP, widely recognized as the reference

method for DNA methylation analysis (Figs. 4N–4O). Analysis revealed that HK-2 cells exposed to PA exhibited aberrant Klotho DNA methylation, which was mitigated by Hed.

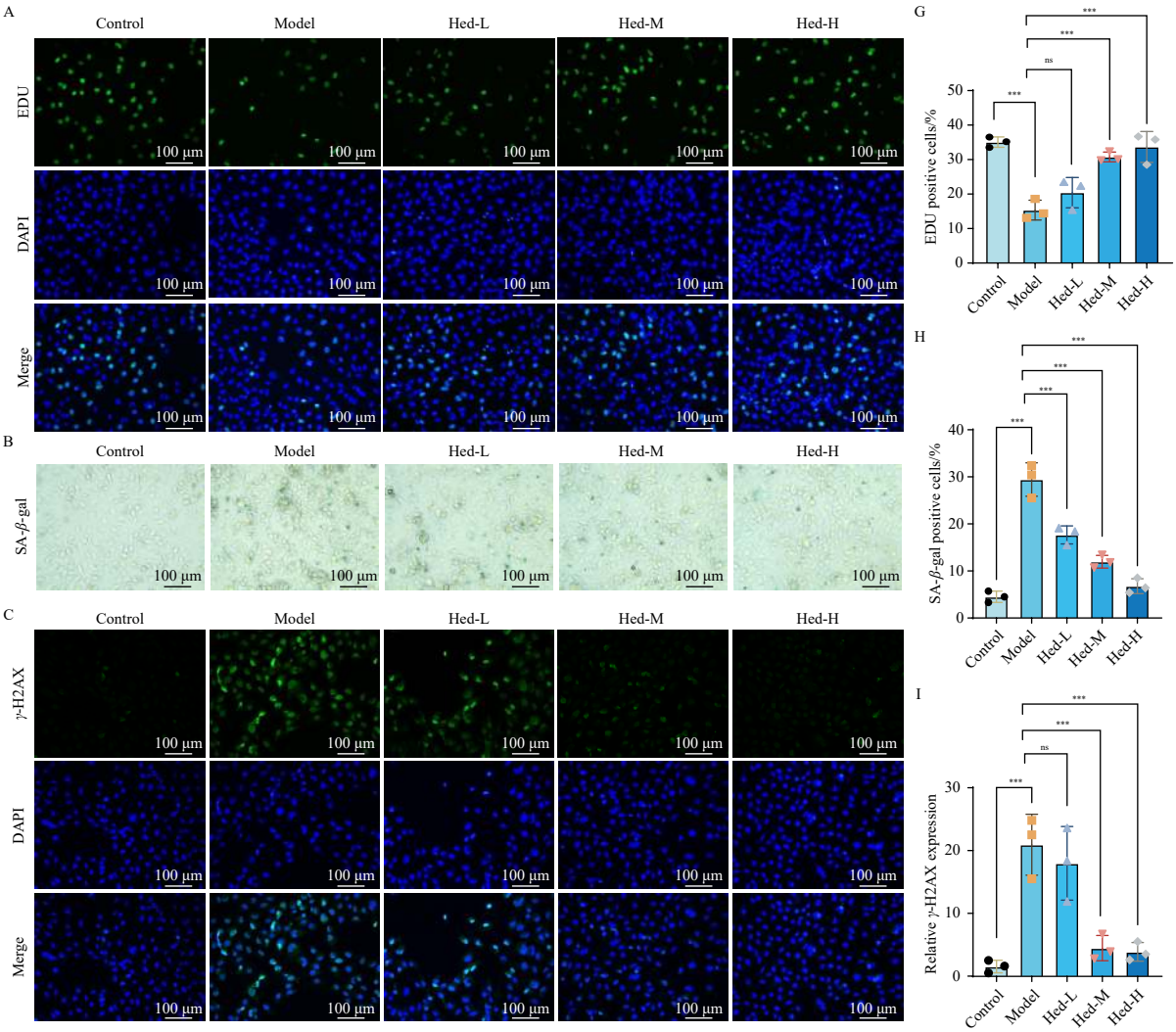
Further analysis of DNA methyltransferase (DNMT) expression revealed that DNMT1 and DNMT3B protein levels rose in parallel with increasing PA concentrations, consistent with DNMT's role in promoting DNA methylation (Figs. 4P–4S). Hed and the DNA methyltransferase inhibitor 5-AZA both lowered DNMT1 protein expression; however, Hed had little effect on DNMT3B levels (Figs. 4T–4V). These findings indicate that, although both DNMT1 and DNMT3B are upregulated in response to PA treatment, DNMT1 represents the primary epigenetic effector targeted by Hed in this cellular context. Consistently, attenuation of Klotho promoter hypermethylation and restoration of Klotho expression following Hed treatment were closely associated with suppression of DNMT1 rather than DNMT3B. Together, these results support a DNMT1-selective mechanism underlying Hed-mediated demethylation of the Klotho promoter in PA-treated HK-2 cells. DNMT1 primarily maintains methylation patterns during DNA replication, whereas DNMT3B is mainly responsible for de novo methylation. The selective targeting of DNMT1 by Hed may therefore be particularly relevant in stress-induced senescence, where aberrant maintenance methylation locks cells into a senescent state. Nevertheless, given the observed induction of DNMT3B by PA, a contributory role of DNMT3B in establishing or maintaining the hypermethylated state of the Klotho promoter cannot be fully excluded. Further studies employing DNMT3B-specific genetic or epigenetic perturbation will be required to delineate its potential involvement in Klotho promoter hypermethylation under PA stress.

3.5. The removal of Klotho DNA hypermethylation is crucial for Hed's anti-renal senescence effects

Reduced Klotho expression due to aberrant hypermethylation of the Klotho gene is a major factor in renal senescence. In the PA-induced senescence model, we sought to clarify how abnormal DNA methylation–mediated Klotho suppression contributes to renal senescence. Figs. 5A, 5F, and 5G demonstrated that 5-AZA restored levels of cell growth. Furthermore, 5-AZA produced a similar effect as Hed treatment in restoring the proportion of cells at the G_2/M phase (Figs. 5D and 5J). Following PA exposure, SA-β-gal-positive cell counts increased markedly, whereas 5-AZA treatment significantly reduced them (Figs. 5B and 5H). In addition, 5-AZA reduced the PA-induced upregulation of P16, P21, and P53 protein expression. Similarly, 5-AZA treatment during PA exposure restored Klotho protein levels while suppressing the levels of additional fibrosis-related proteins (Figs. 5E, 5K–5Q). Figs. 5C and 5I illustrated that treatment with 5-AZA partially mitigated the PA-induced elevation of γ-H2AX levels. The results indicate that Hed's capacity to delay renal senescence is partly attributable to its effect in reducing DNA hypermethylation.

3.6. Hed inhibits aberrant DNA methylation by binding DNMT1 and reducing its occupancy on the Klotho promoter

We dug more into the regulatory implications of the Hed-DN-



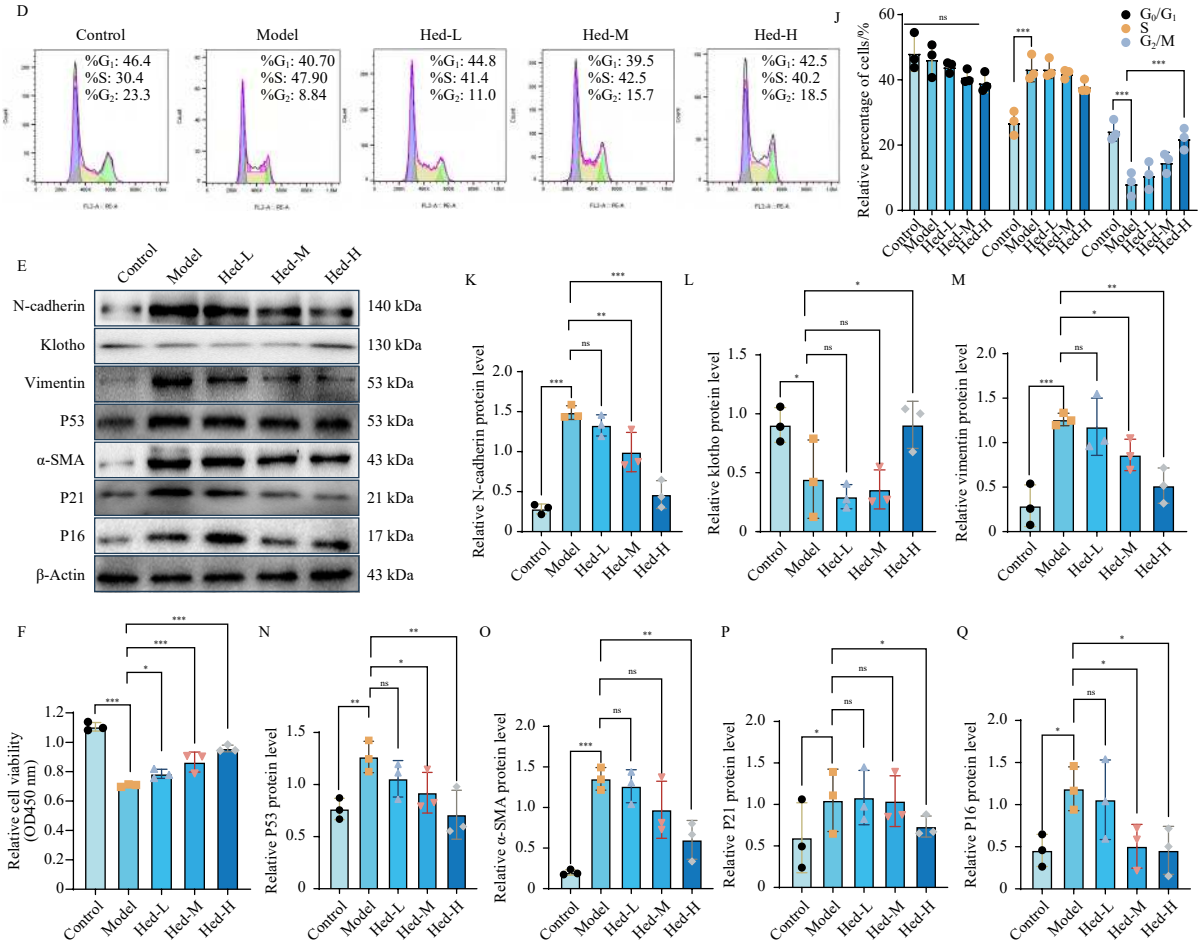


Fig. 2 Hed inhibits HK-2 cell senescence induced by Palmitic acid. (A) Cell proliferation was assessed by EdU assay. (B) Senescence-associated β-galactosidase staining. (C) Immunofluorescence detection of DNA damage marker γ-H2AX expression. (D) The cell cycle of HK-2 treated with Hed was measured by flow cytometry. (E) Western blot analysis. (F) CCK-8 quantification results of HK-2 after Hed treatment. (G) EdU staining quantification results of HK-2 after Hed treatment. (H) senescence-associated *β*-galactosidase staining quantification results of HK-2 after Hed treatment. (I) Immunofluorescence quantification results of HK-2 after Hed treatment. (J) Cell cycle quantification results of HK-2 after Hed treatment. (K–Q) Western blot quantification results of N-cadherin, Klotho, Vimentin, P53, α-SMA, P21 and P16. Data are presented as mean ± SD and statistical analysis was performed using one-way ANOVA followed by LSD post hoc test (n = 3 each, experiments performed in triplicate). $^{*}P < 0.05$, $^{**}P < 0.01$, $^{***}P < 0.001$, NS, not significant. All microscopic images were captured at × 20 magnification. Scale bar = 100 μm.

MT1 interaction on DNA methylation in Klotho. The anticipated interaction conformation between DNMT1 and Hed was displayed in Fig. 6A. According to molecular docking experiments, Hed had a –8.8 kcal·mol^{-1} relative energy interaction with six DNMT1 amino acid residues: CYS-653, ASN-1529, THR-1528, GLN-1536, LYS-697, and LYS-1535. The initial configuration for the MD simulation was derived from the optimized Hed-DNMT1 complex structure. Fig. 6B presents a surface representation of the Hed–DNMT1 complex. Throughout the MD simulation, Hed remained stably positioned at the core of the DNMT1 binding pocket. During the molecular dynamics simulation, RMSD analysis of Hed indicated stable oscillations around 0.25 Å from 0 to 100 ns, while the all-atom RMSD of DNMT1 exhibited minor fluctuations near 2 Å throughout the simulation (Fig. 6C). We employed SPR to monitor real-time interactions and further characterize the binding between Hed and DNMT1. The interaction between Hed and DNMT1 was studied using a 3D dextran sensor chip, allowing assessment of binding kinetics and affinity. SPR imaging showed that Hed and DNMT1 had a substantial binding capacity, as indicated by an equilibrium dissociation constant (KD) of 1.23×10^{-5} mol·L^{-1} (Fig. 6D). The observed KD for Hed binding to DNMT1 falls within the micromolar range reported for other non-nucleoside DNMT1 inhibitors. For example, RG108, a commonly used small-molecule DNMT inhibitor, reported DNMT inhibitory activity in the micromolar range [20]. Similarly, SGI-1027 has been shown to inhibit DNMT activity, including DNMT1, with IC50 values in the low-micromolar range in biochemical assays [21]. CETSA and DARTS assays were additionally used to characterize how Hed engages with DNMT1. DNMT1 demonstrated a notable increase in thermal stability after being treated with Hed, according to the CETSA data (Figs. 6E–6F). Also, the DARTS data showed that Hed greatly improved the stability of DNMT1 when subjected to degradation by pronase (Figs. 6G–6H). ChIP-qPCR experiments were performed (Fig. 6I). The results suggested that Hed treatment reduced the association of DNMT1 with the Klotho promoter. To further validate the direct interaction between DNMT1 and the Klotho promoter, electrophoretic mobility shift assays (EMSA) were performed. DNMT1 markedly increased the formation of DNA-protein complexes, whereas Hed treatment significantly attenuated the DNMT1-DNA binding signal, similar to the effect observed with the DNMT1 inhibitor 5-AZA (Fig. 6J). Consistently, DNA pull-down assays demonstrated that DNMT1 directly bound to the Klotho promoter fragment, and this interaction was substantially reduced upon Hed or 5-AZA treatment (Fig. 6K). Collectively, the data suggest that Hed disrupts DNMT1 binding to the Klotho promoter by directly interfering with DNMT1-DNA interactions.

3.7. DNMT1 is critically involved in PA-induced senescence during Hed treatment

DNMT1 expression was either silenced or enhanced in HK-2

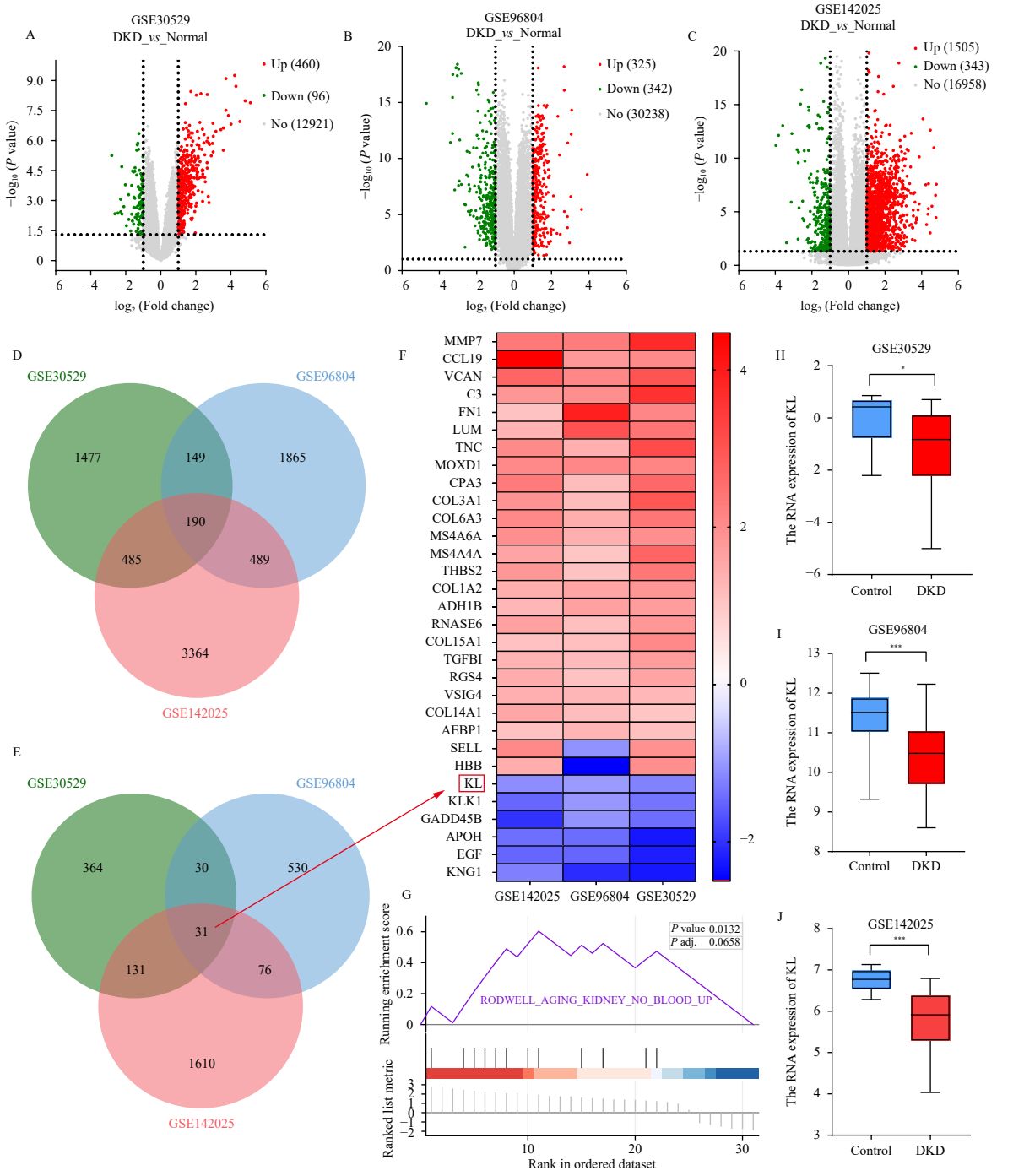


Fig. 3 Identification of DEGs and functional enrichment analyses. (A–C) Volcano plot of GSE30529, GSE96804, GSE142025. (D) Venn diagrams of DEGs, log FC > 0 or log FC < 0. (E) Venn diagrams of DEGs, log FC > 1 or log FC < −1. (F) Differential gene heat map. (G) GSEA pathway enrichment analysis results. (H–J) Klotho expression in the GSE30529, GSE96804, GSE142025. $^{*}P < 0.05$, $^{**}P < 0.01$, $^{***}P < 0.001$, NS, not significant.

cells to determine whether Hed's anti-senescence effects are dependent on DNMT1. Cell proliferation was restored by DNMT1 siRNA treatment, as demonstrated in Figs. S3a and S3f–S3g. Following DNMT1 siRNA administration, the percentage of cells residing in the G_2/M phase was elevated (Figs. S3d and S3j). PA-induced increases in SA-β-gal-positive cells were substantially attenuated by DNMT1 knockdown (Figs. S3b and S3h). Additionally, DNMT1 siRNA reduced the PA-induced increase in senescence markers such as P16, P21, and P53. Klotho protein expression was also recovered by DNMT1 siRNA treatment (Figs. S3e, S3k–S3n). Additionally, Figs. S3c and S3i illustrate that the PA-induced increase in γ-H2AX was partially alleviated by DNMT1 siRNA treatment. The data indicate that DNMT1 knockdown reduces stress senescence caused by PA.

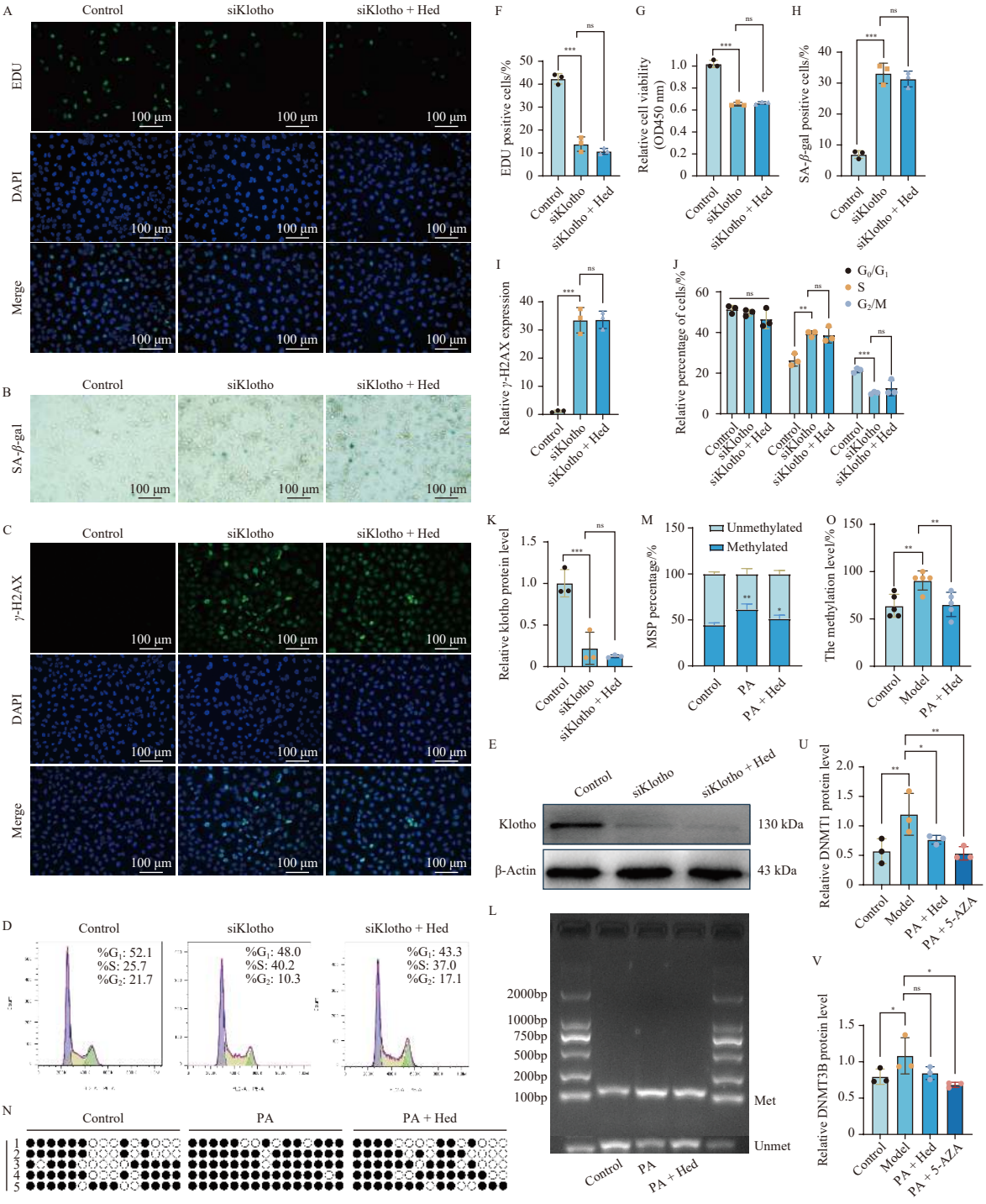
Subsequently, we examined how Hed regulates DNMT1 by inducing DNMT1 overexpression. Figs. 7A and 7F–7g indicated that DNMT1 overexpression inhibited cell proliferation, which was inhibited by Hed treatment. Figs. 7D and 7J showed that Hed treatment recovered the G_2/M phase cell population. Figs. 7B and 7H showed that DNMT1 overexpression markedly elevated SA-β-gal-positive cell counts, whereas Hed treatment substantially reduced them. Moreover, data presented in Figs. 7E and 7K–7N indicated that Hed restored Klotho protein levels while suppressing P16, P21, and P53 expression. Furthermore, as demonstrated in Figs. 7C and 7I, Hed had a modest ameliorative effect on the elevated γ-H2AX levels in cells overexpressing DNMT1. Finally, DN-

MT1 is a key target for Hed's suppression of renal senescence, and Hed successfully alleviates stressed senescence due to DNMT1 overexpression.

4. Discussion

Cellular senescence has emerged as a central driver of diabetic kidney disease progression rather than a passive consequence of metabolic injury. In this study, we identify hederagenin as a novel epigenetic modulator that counteracts renal senescence by restoring Klotho expression through inhibition of DNMT1-mediated DNA methylation. Mechanistically, Hed binds to DNMT1, inhibiting its interaction with the Klotho promoter, which leads to a reduction in DNA methylation at this site. This results in the upregulation of Klotho, a gene that counteracts cellular senescence, reduces DNA lesions, and slows the progression of renal aging.

Our study's most important discovery is that Klotho is an essential component of Hed's treatment for renal senescence. Klotho is widely recognized as an anti-aging protein. Radiation-induced senescence of renal epithelial cells involves Klotho-associated pathways, and exposure to polystyrene microplastics accelerates tubular epithelial cell senescence, leading to renal fibrosis. Thus, reduced Klotho activity may enhance environmentally induced tubular epithelial cell senescence, whereas preservation of Klotho may confer protection against renal fibrogenesis [22,23]. Klotho further mitigates the progression of renal fibrosis by maintaining mitochondrial integrity and restricting senescence in tubular epithelial cells [24]. Cells undergo premature senescence as DKD progresses, setting off a cascade of events that promote inflammation and fibrosis [25]. Although Klotho's involve-



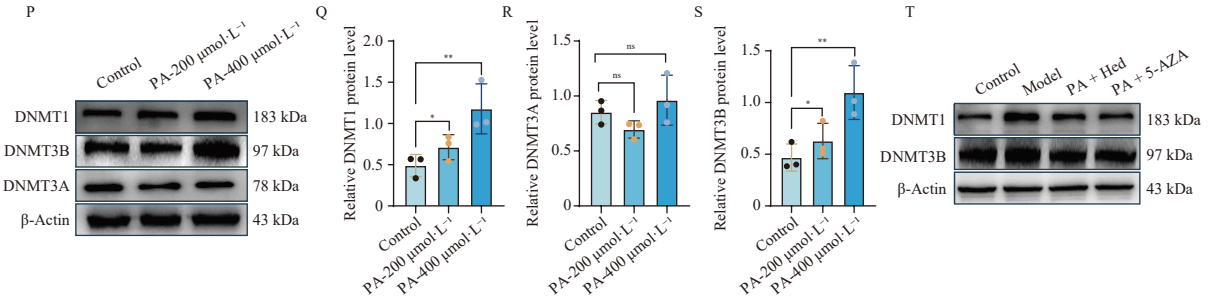


Fig. 4 Klotho plays a critical role in Hed-mediated inhibition of senescence. (A) Cell proliferation was assessed by EdU assay. (B) Senescence-associated β-galactosidase staining. (C) Immunofluorescence detection of DNA damage marker γ-H2AX expression. (D) The cell cycle of HK-2 treated with siKlotho was measured by flow cytometry. (E) Western blot analysis. (F) EdU staining quantification results of HK-2 after siKlotho treatment. (G) CCK-8 quantification results of HK-2 after siKlotho treatment. (H) senescence-associated β-galactosidase staining quantification results of HK-2 after siKlotho treatment. (I) Immunofluorescence quantification results of HK-2 after siKlotho treatment. (J) Cell cycle quantification results of HK-2 after siklotho treatment. (K) Western blot quantification results of Klotho. (L–M) Methylation-specific PCR and quantification results of the Klotho promoter region was performed on HK-2 cell. (N–O) Bisulfite sequencing analysis and quantification of the Klotho promoter in HK-2 cells. (P–S) Western blot analysis and quantification results of DNMT1, DNMT3B, DNMT3A. (T–V) Western blot analysis and quantification results of DNMT1, DNMT3B. Data are presented as mean ± SD and statistical analysis was performed using one-way ANOVA followed by LSD post hoc test (n = 3 each, experiments performed in triplicate). $^{*}P < 0.05$, $^{**}P < 0.01$, $^{***}P < 0.001$, NS, not significant. All microscopic images were captured at × 20 magnification. Scale bar = 100 μm.

ment in DKD is well documented, its epigenetic regulation in this context remains poorly understood. Bioinformatics analysis of the GEO database revealed reduced Klotho levels in DKD (Fig. 3). Earlier studies reported 30%–40% methylation of the Klotho promoter in Klotho-silenced cells, whereas the promoter is largely unmethylated in Klotho-expressing renal tubular cells. Demethylation treatment increased Klotho expression 1.5–3.0 fold and reactivated previously silenced reporter constructs [26]. Increased methylation of the Klotho promoter, which reduces Klotho expression, has been reported in both animal models of kidney disease [27-29] and human patients [30]. In DKD, the Klotho promoter exhibits pronounced hypermethylation, which is effectively reversed by Hed treatment. This restoration of Klotho expression contributes to the attenuation of renal injury and cellular senescence (Figs. 4–5). Although the reduction in average DNA methylation of the Klotho promoter (about 5%) appears modest, it is important to note that transcriptional regulation is often driven by site-specific CpG changes rather than global methylation levels. Small changes at critical CpG sites can substantially alter transcription factor accessibility and chromatin structure. Moreover, our ChIP-qPCR and EMSA results demonstrated that hederagenin markedly reduced DNMT1 occupancy and DNA-binding activity at the Klotho promoter, suggesting that disruption of DNMT1-mediated transcriptional repression, rather than bulk methylation changes alone, plays a dominant role in reactivating Klotho expression. To ensure that the observed effects were due to pharmacological activity rather than non-specific cytotoxicity, we conducted CCK-8 cell viability assays prior to the *in vitro* experiments. These results confirmed that Hed at concentrations up to 50 μmol·L^{-1} did not induce cytotoxicity in HK-2 cells. Therefore, the selected concentrations (12.5, 25, and 50 μmol·L^{-1}) were safe and appropriate for studying its anti-senescence effects (Fig. S4). Overall, these results indicate that Klotho is involved in Hed-mediated protection against renal senescence, with promoter DNA methylation serving as a key regulatory mechanism in DKD. These findings also align with the broader direction of natural product research in renal fibrosis, which increasingly connects traditional ethnopharmacological knowledge with modern mechanistic studies [31].

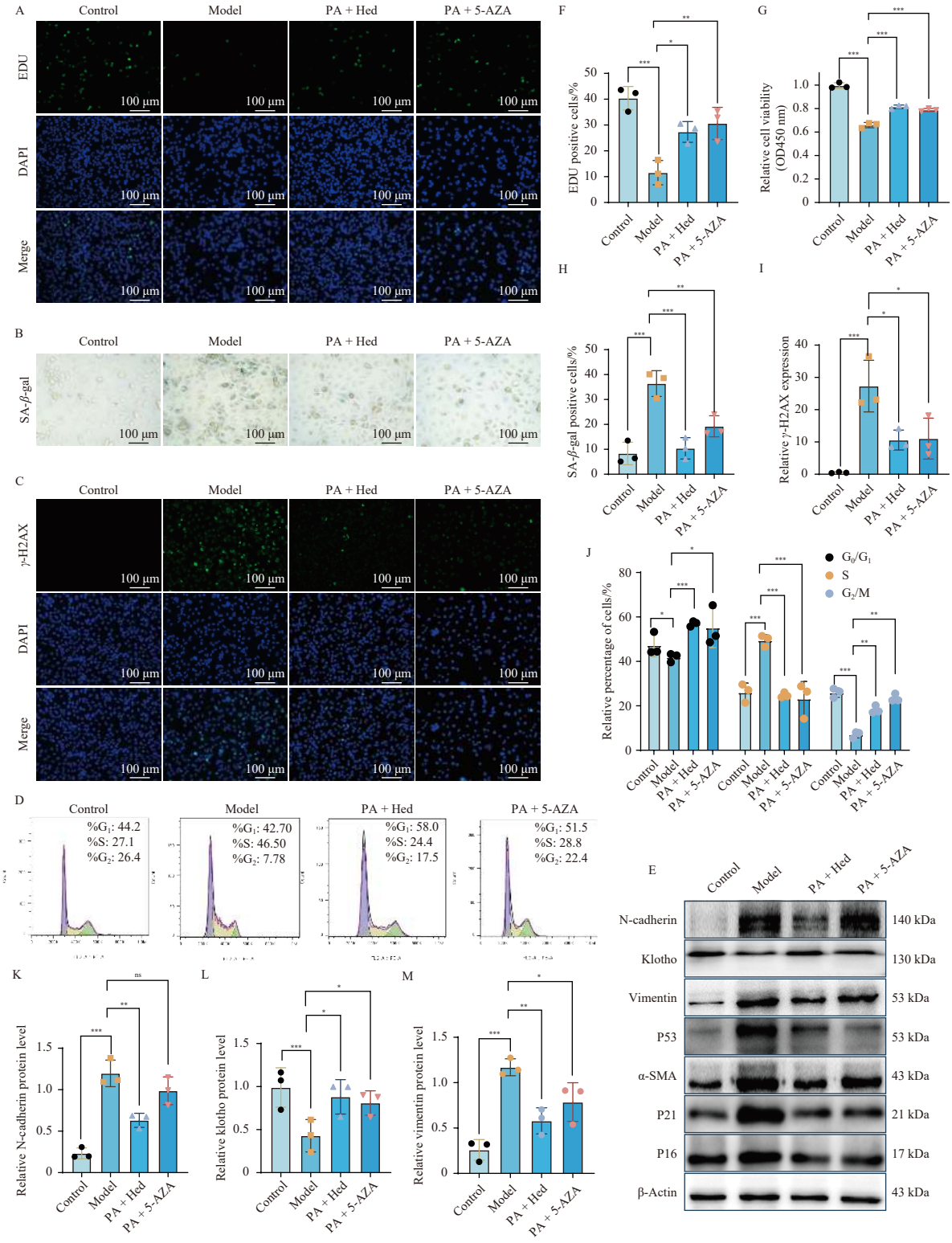
Consistent with this notion, accumulating evidence indicates that pathological stimuli can trigger epigenetic reprogramming, thereby accelerating the progression of renal disorders [32-34]. Accordingly, targeting DNA methylation has emerged as a potentially viable therapeutic strategy for DKD. Decitabine, or 5-aza-2'-deoxycytidine, is a popular deoxycytidine analog for promoter demethylation-mediated activation of methylated and silenced genes [35]. As a widely recognized technique, this method facilitates the study of DNA methylation-related characteristics in both human and animal tissues [36-38]. As an essential modulator of DNA methylation, DNMT1 expression changes can reshape methylation landscapes, thereby impacting the expression of downstream genes [39]. Prior investigations indicate that DNMT1 functions as a key mediator in DKD, affecting both disease progression and its regulatory mechanisms. For instance, treatment with Cissus quadrangularis extract, which modulates the SIRT1/DNMT1 pathway, alleviates diabetic nephropathy in rats given a high-fat diet followed by streptozotocin injection [40]. Podocyte injury in db/db mice can be alleviated by DNA methylation inhibitors, which act through modulation of the Sp1/NF-κB p65-DNMT1 signaling axis [41]. In addition, multiple clinical studies have examined DNMT1, underscoring its significance as an indicator and therapeutic target in human DKD [42-44]. Using MSP, BSP, and Western blot techniques, we observed that Hed treatment downregulated DNMT1, lowered the methylation status of the Klotho promoter, and consequently elevated Klotho expression. Furthermore, molecular docking, SPR, ChIP-qPCR, EMSA and DNA pull down analyses revealed that Hed interacts with DNMT1, restricting its binding to the Klotho promoter (Fig. 6), thereby lowering promoter methylation. Evidence from this study indicates that DNMT1 mediates Hed's pharmacological effects, reducing senescence and DNA damage in DKD. Consequently, DNMT1 is suggested as a potential target through which Hed modulates DNA methylation to counteract DKD.

While our data strongly support DNMT1 as a primary molecular target of Hed, the observation that Hed partially alleviated senescence even under DNMT1 overexpression conditions suggests that additional mechanisms may also contribute to its renoprotective effects. This finding highlights the complexity of Hed's mode of action and warrants further investigation to fully elucidate its broader regulatory network in renal senescence.

Although our findings highlight the effectiveness of Hed in DKD, several limitations should be noted. First, although we used three different doses of Hed (2.5, 5, and 10 mg·kg^{-1}) in the db/db mouse model and observed dose-dependent efficacy without significant toxicity, consistent with previous reports, the optimal therapeutic dose and safety margin for Hed remain to be fully elucidated. To date, there have been no reports of human fatalities due to Hed. During acute toxicity testing in mice, no signs of toxicity or deaths were observed, and oral administration of Hed was tolerated at doses exceeding 20 g·kg^{-1} [45]. Hederagenin has been reported to exhibit relatively low toxicity *in vivo*, with no significant liver or kidney damage observed in experimental models [46] In another study, 50 mg·kg^{-1}Hed was shown to improve cognitive impairment and renal fibrosis in DKD without observing any toxicity [9, 47]. However, there is evidence suggesting that Hed might exhibit potential toxicity in animal species other

than rats and mice. Reports from France have indicated that Hed may be toxic to cows and horses [48]. These discrepancies highlight the complex relationship between dose, efficacy, and toxicity, which may vary depending on factors such as animal species, target tissues, disease models, dosing frequency, and treatment duration. Comprehensive dose-response and toxicological studies are needed to establish a safe and effective Hed dosing regimen for clinical use.

Second, while our study provides promising preclinical evidence, several limitations should be acknowledged. In this study, mechanistic investigations were primarily performed in HK-2 cells and mouse models, and the effects of Hed have not yet been validated in primary human renal tubular epithelial cells. Therefore, future investigations involving primary human cells and additional translational models are required to validate the applicability of our findings to human DKD. The translational potential of Hed for the treatment of DKD in humans remains unexplored. The clinical significance of the observed effects warrants careful evaluation. Future studies should conduct clinical trials to evaluate Hed's therapeutic effects and tolerability in human subjects, with careful monitoring for adverse reactions. These studies should also aim to identify the optimal therapeutic dose for hu-



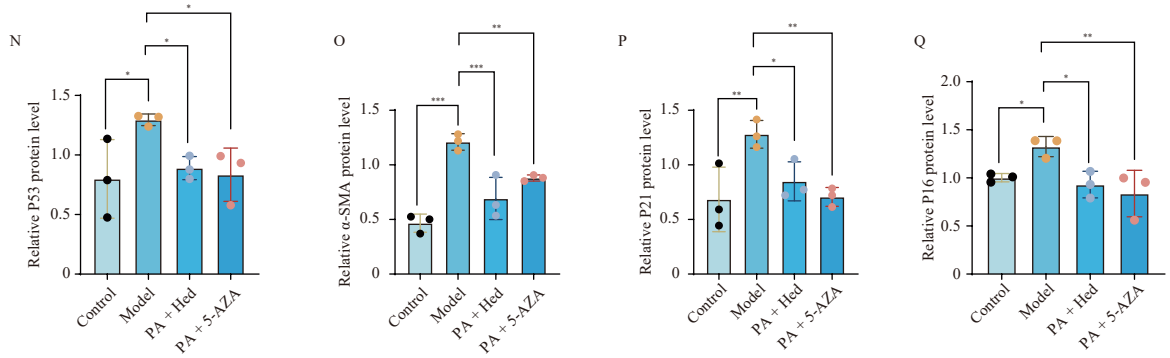


Fig. 5 Elimination of Klotho DNA hypermethylation is essential for the anti-renal senescence effects of Hed. (A) Cell proliferation was assessed by EdU assay. (B) Senescence-associated β-galactosidase staining. (C) Immunofluorescence detection of DNA damage marker γ-H2AX expression. (D) The cell cycle of HK-2 treated with 5-AZA was measured by flow cytometry. (E) Western blot analysis. (F) EdU staining quantification results of HK-2 after 5-AZA treatment. (G) CCK-8 quantification results of HK-2 after 5-AZA treatment. (H) senescence-associated *β*-galactosidase staining quantification results of HK-2 after 5-AZA treatment. (I) Immunofluorescence quantification results of HK-2 after 5-AZA treatment. (J) Cell cycle quantification results of HK-2 after 5-AZA treatment. (K–Q) Western blot quantification results of N-cadherin, Klotho, Vimentin, P53, α-SMA, P21 and P16. Data are presented as mean ± SD and statistical analysis was performed using one-way ANOVA followed by LSD post hoc test (n = 3 each, experiments performed in triplicate). $^{*}P < 0.05$, $^{**}P < 0.01$, $^{***}P < 0.001$, NS, not significant. All microscopic images were captured at × 20 magnification. Scale bar = 100 μm.

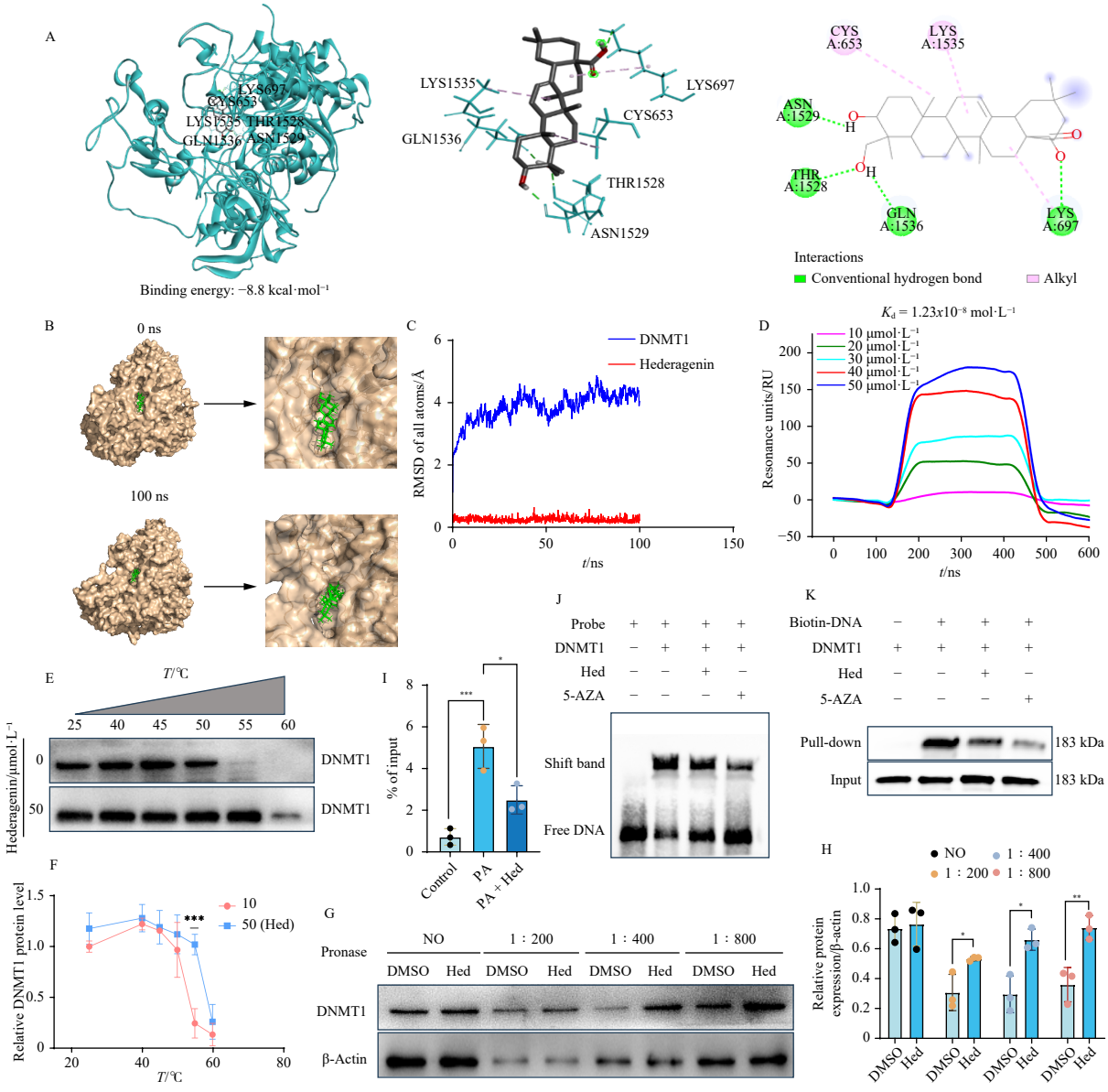


Fig. 6 Hed binds DNMT1 and reduces its occupancy on the Klotho promoter. (A) Molecular docking of DNMT1 and Hed. (B) Surface visualization models of the Hed-DNMT1 complex at 0 and 100 ns. (C) Plots of root mean square deviation of all atoms of DNMT1 (blue) and Hed (red). (D) SPRi fitting curves for Hed to DNMT1. (E–F) CETSA-Western blot analysis showed the protection of DNMT1 by Hed at different temperature gradients. (G–H) DARTS-Western blot analysis showed the resistance of DNMT1 to pronase digestion under the treatment of Hed. (I) ChIP-qPCR results. (J) EMSA analysis of DNMT1 binding to the Klotho promoter. (K) DNA pull-down assay of DNMT1 binding to the Klotho promoter. Data are presented as mean ± SD and statistical analysis was performed using one-way ANOVA followed by LSD post hoc test (n = 3 each, experiments performed in triplicate). $^{*}P < 0.05$, $^{**}P < 0.01$, $^{***}P < 0.001$, NS, not significant.

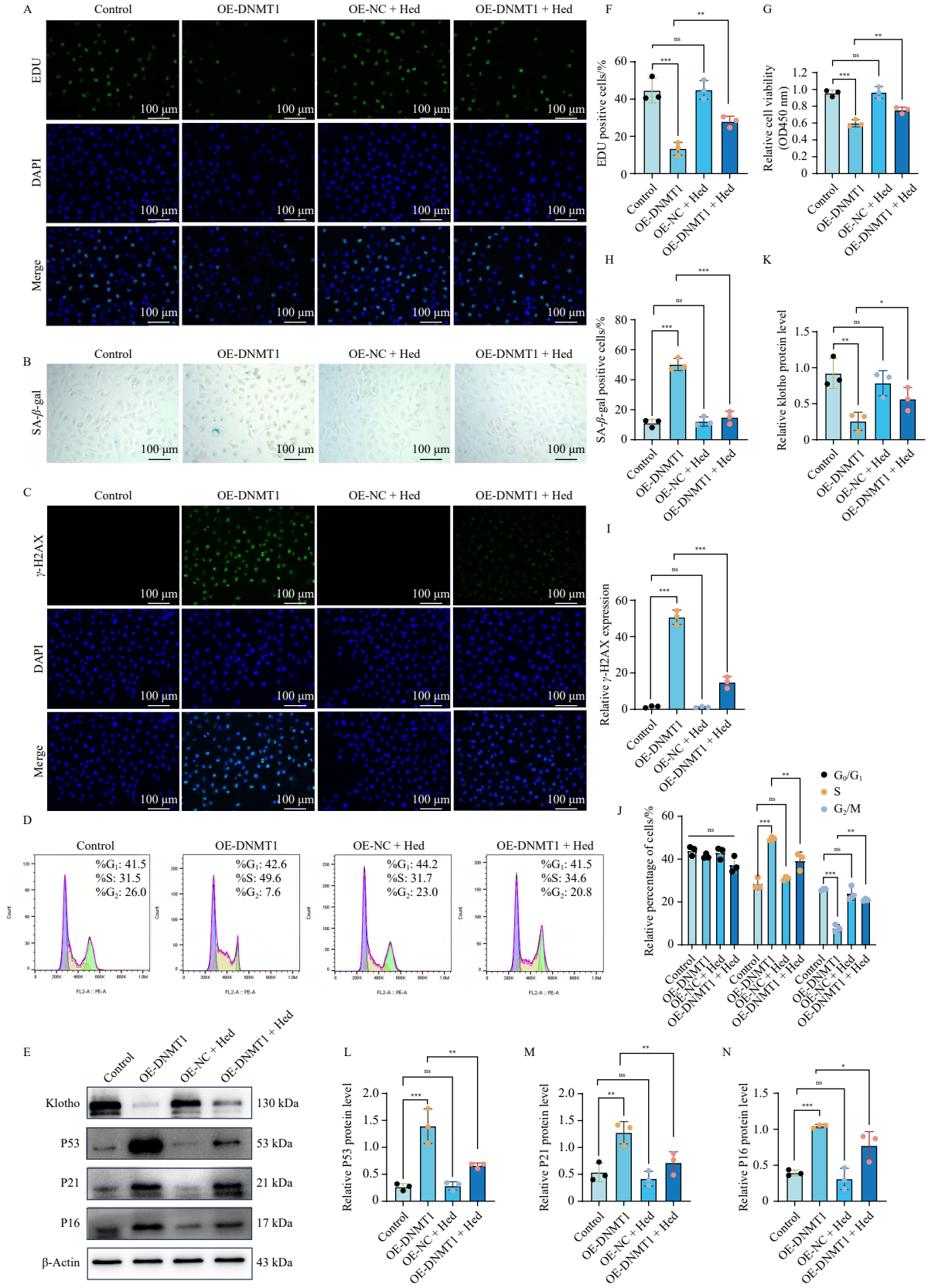


Fig. 7 Effect of overexpression of DNMT1 in the treatment of stressful senescence by Hed. (A) Cell proliferation was assessed by EdU assay. (B) Senescence-associated β-galactosidase staining. (C) Immunofluorescence detection of DNA damage marker γ-H2AX expression. (D) The cell cycle was measured by flow cytometry. (E) Western blot analysis. (F) EdU staining quantification results. (G) CCK-8 quantification results. (H) senescence-associated β-galactosidase staining quantification results. (I) Immunofluorescence quantification results. (J) Cell cycle quantification results. (K–N) Western blot quantification results of Klotho, P53, P21 and P16. Data are presented as mean ± SD and statistical analysis was performed using one-way ANOVA followed by LSD post hoc test (n = 3 each, experiments performed in triplicate). $^{*}P < 0.05$, $^{**}P < 0.01$, $^{***}P < 0.001$, NS, not significant. All microscopic images were captured at × 20 magnification. Scale bar = 100 μm.

mans, which may differ from the doses used in our animal models. Furthermore, studies on drug interactions and long-term safety will be essential to assess whether Hed can be safely and effectively applied in DKD treatment.

This study provides compelling evidence that Hed ameliorates diabetic kidney disease through inhibition of DNMT1-driven hypermethylation at the Klotho promoter. A prior version of this work was publicly posted as a preprint on Research Square. The preprint has not been peer-reviewed and has now been properly cited for transparency.

5. Conclusion

This work suggests that Hed attenuates renal senescence in DKD by epigenetically restoring Klotho expression. Mechanistically, Hed interacts with DNMT1 and reduces its occupancy at the Klotho promoter, leading to decreased promoter methylation and reactivation of Klotho's anti-senescent function. As a result, downstream injury responses are dampened and renal cellular senescence is alleviated. Collectively, these data support Hed as a promising therapeutic candidate and reinforce the protective role of Klotho in DKD. Taken together, our findings position Hed as an epigenetic modulator with translational relevance for senescence-driven diabetic kidney disease.

Funding

This work was supported by the National Natural Science Foundation of China (Nos. 82274510, 82474454, 82405070, 82360918), the Natural Science Foundation of Guangdong Province, China (No. 2024A1515012173), and the Jiangxi Provincial Administration of Traditional Chinese Medicine Science and Technology Plan (No. 2023B0597).

Declaration of competing interest

These authors have no conflict of interest to declare.

Data availability

Data will be available on request by sending E-mail to the corresponding authors.

References

1 Tuttle KR, Agarwal R, Alpers CE, et al. Molecular mechanisms and therapeutic targets for diabetic kidney disease. *Kidney Int*. 2022;102(2):248-260. https://doi.org/10.1016/j.kint.2022.05.012.
2 Umanath K, Lewis JB. Update on diabetic nephropathy: core curriculum 2018. *Am J Kidney Dis*. 2018;71(6):884-895. https://doi.org/10.1053/j.ajkd.2017.10.026.
3 Perkovic V, Jardine MJ, Neal B, et al. Canagliflozin and renal outcomes in type 2 diabetes and nephropathy. *N Engl J Med*. 2019;380(24):2295-2306. https://doi.org/10.1056/NEJMoa1811744.
4 Liu MN, Li XL, Gao YH, et al. Breaking the fibrotic code: nanotechnology-driven advances in renal fibrosis therapy. *Biomaterials*. 2026;327:123738. https://doi.org/10.1016/j.biomaterials.2025.123738.
5 Zhang HZ, Li Y, Liu Y. An updated review of the pharmacological effects and potential mechanisms of hederagenin and its derivatives. *Front Pharmacol*. 2024;15:1374264. https://doi.org/10.3389/fphar.2024.1374264.
6 Xie KH, Liu XH, Jia J, et al. Hederagenin ameliorates cisplatin-induced acute kidney injury *via* inhibiting long non-coding RNA A330074k22Rik/Axin2/β-catenin signalling pathway. *Int Immunopharmacol*. 2022;112:109247. https://doi.org/10.1016/j.intimp.2022.109247.
7 Jia J, Xu LH, Deng C, et al. Hederagenin ameliorates renal fibrosis in chronic kidney disease through blocking ISG15 regulated JAK/STAT signaling. *Int Immunopharmacol*. 2023;118:110122. https://doi.org/10.1016/j.intimp.2023.110122.
8 Yang W, He LJ. The protective effect of hederagenin on renal fibrosis by targeting muscarinic acetylcholine receptor. *Bioengineered*. 2022;13(4):8689-8698. https://doi.org/10.1080/21655979.2022.2054596.
9 Jia J, Tan RZ, Xu LH, et al. Hederagenin improves renal fibrosis in diabetic nephropathy by regulating Smad3/NOX4/SLC7A11 signaling-mediated tubular cell ferroptosis. *Int Immunopharmacol*. 2024;135:112303. https://doi.org/10.1016/j.intimp.2024.112303.
10 Yang GH, Yang W, Jiang HR, et al. Hederagenin inhibits high glucose-induced fibrosis in human renal cells by suppression of NLRP3 inflammasome activation through reducing cathepsin B expression. *Chem Biol Drug Des*. 2023;102(6):1409-1420. https://doi.org/10.1111/cbdd.14332.
11 Liu TL, Li XL, Chen YD, et al. Natural products in treating diabetic kidney disease: a visualized bibliometric analysis. *Front Pharmacol*. 2025;16:1522074. https://doi.org/10.3389/fphar.2025.1522074.
12 Schubeler D. Function and information content of DNA methylation. *Nature*. 2015;517(7534):321-326. https://doi.org/10.1038/nature14192.
13 Akhouri V, Majumder S, Gaikwad AB. Targeting DNA methylation in diabetic kidney disease: a new perspective. *Life Sci*. 2023;335:122256. https://doi.org/10.1016/j.lfs.2023.122256.
14 Gao Q, Chen F, Zhang LJ, et al. Inhibition of DNA methyltransferase aberrations reinstates antioxidant aging suppressors and ameliorates renal aging. *Aging Cell*. 2022;21(1):e13526. https://doi.org/10.1111/acel.13526.
15 Jiang W, Gan C, Zhou XD, et al. Klotho inhibits renal ox-LDL deposition *via* IGF-1R/RAC1/OLR1 signaling to ameliorate podocyte injury in diabetic kidney disease. *Cardiovasc Diabetol*. 2023;22(1):293. https://doi.org/10.1186/s12933-023-02025-w.
16 Kim SS, Song SH, Kim IJ, et al. Decreased plasma alpha-Klotho predict progression of nephropathy with type 2 diabetic patients. *J Diabetes Complicat*. 2016;30(5):887-892. https://doi.org/10.1016/j.jdiacomp.2016.03.006.
17 Lee EY, Kim SS, Lee JS, et al. Soluble α-klotho as a novel biomarker in the early stage of nephropathy in patients with type 2 diabetes. *PLoS One*. 2014;9(8):e102984. https://doi.org/10.1371/journal.pone.0102984.
18 Chen GH, Xu HL, Wu YT, et al. Myricetin suppresses the proliferation and migration of vascular smooth muscle cells and inhibits neointimal hyperplasia *via* suppressing TGFBR1 signaling pathways. *Phytomedicine*. 2021;92:153719. https://doi.org/10.1016/j.phymed.2021.153719.
19 Bird A. DNA methylation patterns and epigenetic memory. *Genes Dev*. 2002;16(1):6-21. https://doi.org/10.1101/gad.947102.
20 Brueckner B, Garcia Boy R, Siedlecki P, et al. Epigenetic reactivation of tumor suppressor genes by a novel small-molecule inhibitor of human DNA methyltransferases. *Cancer Res*. 2005;65(14):6305-6311. https://doi.org/10.1158/0008-5472.CAN-04-2957.
21 Gros C, Fleury L, Nahoum V, et al. New insights on the mechanism of quinoline-based DNA Methyltransferase inhibitors. *J Biol Chem*. 2015;290(10):6293-6302. https://doi.org/10.1074/jbc.M114.594671.
22 Pan C, Wang XL, Fan ZC, et al. Polystyrene microplastics facilitate renal fibrosis through accelerating tubular epithelial cell senescence. *Food Chem Toxicol*. 2024;191:114888. https://doi.org/10.1016/j.fct.2024.114888.
23 Kim DY, Lee M, Kim EJ. Involvement of Klotho, TNF-α; and ADAMs in radiation-induced senescence of renal epithelial cells. *Mol Med Rep*. 2021;23(1):22. doi:10.3892/mmr.2020.11660
24 Miao JH, Huang JW, Luo CW, et al. Klotho retards renal fibrosis through targeting mitochondrial dysfunction and cellular senescence in renal tubular cells. *Physiol Rep*. 2021;9(2):e14696. https://doi.org/10.14814/phy2.14696.
25 Typiak M, Piwkowska A. Antiinflammatory actions of Klotho: implications for therapy of diabetic nephropathy. *Int J Mol Sci*. 2021;22(2):956. doi:10.3390/ijms22020956
26 Azuma M, Koyama D, Kikuchi J, et al. Promoter methylation confers kidney-specific expression of the Klotho gene. *FASEB J*. 2012;26(10):4264-4274. https://doi.org/10.1096/fj.12-211631.
27 Yin SS, Zhang Q, Yang J, et al. TGFβ-incurred epigenetic aberrations of miRNA and DNA methyltransferase suppress Klotho and potentiate renal fibrosis. *Biochim Biophys Acta Mol Cell Res*. 2017;1864(7):1207-1216. https://doi.org/10.1016/j.bbamcr.2017.03.002.
28 Li YN, Chen F, Wei A, et al. Klotho recovery by genistein *via* promoter histone acetylation and DNA demethylation mitigates renal fibrosis in mice. *J Mol Med (Berl)*. 2019;97(4):541-552. https://doi.org/10.1007/s00109-019-01759-z.
29 Zhang Q, Liu L, Lin WJ, et al. Rhein reverses Klotho repression *via* promoter demethylation and protects against kidney and bone injuries in mice with chronic kidney disease. *Kidney Int*. 2017;91(1):144-156. https://doi.org/10.1016/j.kint.2016.07.040.
30 Yu DM, Zhang LE, Yu GQ, et al. Association of liver and kidney functions with Klotho gene methylation in a population environment exposed to cadmium in China. *Int J Environ Health Res*. 2020;30(1):38-48. https://doi.org/10.1080/09603123.2019.1572106.
31 Liu MN, Li XL, Zhang L, et al. Rhubarb in renal fibrosis: from traditional ethnopharmacology to mechanistic therapeutic development. *Chin J Nat Med*. 2026;24(5):526-542. doi:10.1016/S1875-5364(25)60947-2
32 Sarwar MS, Cheng D, Peter RM, et al. Metabolic rewiring and epigenetic reprogramming in leptin receptor-deficient db/db diabetic nephropathy mice. *Eur J Pharmacol*. 2023;953:175866. https://doi.org/10.1016/j.ejphar.2023.175866.
33 Yu ZH, Xu ZY, Liang Y, et al. Vitamin C deficiency causes cell type-specific epigenetic reprogramming and acute tubular necrosis in a mouse model. *J Am Soc Nephrol*. 2022;33(3):531-546. https://doi.org/10.1681/ASN.2021070881.
34 Ouyang L, Su XY, Li WX, et al. ALKBH1-demethylated DNA N6-methyladenine modification triggers vascular calcification *via* osteogenic reprogramming in chronic kidney disease. *J Clin Invest*. 2021;131(14):e146985. doi:10.1172/JCI146985
35 Seelan RS, Mukhopadhyay P, Pisano MM, et al. Effects of 5-aza-2'-deoxycytidine (decitabine) on gene expression. *Drug Metab Rev*. 2018;50(2):193-207. https://doi.org/10.1080/03602532.2018.1437446.
36 Kim DY, Cheong HT, Ra CS, et al. Effect of 5-azacytidine (5-aza) on UCP2 expression in human liver and colon cancer cells. *Int J Med Sci*. 2021;18(10):2176-2186. https://doi.org/10.7150/ijms.56564.
37 Bertoli RM, Chung YJ, Difilippantonio MJ, et al. The DNA methyltransferase inhibitor 5-aza-4'-thio-2'-deoxycytidine induces C > G transversions and

acute lymphoid leukemia development. *Cancer Res*. 2024;84(15):2518-2532. https://doi.org/10.1158/0008-5472.CAN-23-2785.

38 Zhao X, Ruan ZY, Qin XL, et al. The role of 5-aza-2'-deoxycytidine on methylation status of Xist gene in different genders of buffalo (*Bubalus bubalis*) bone marrow mesenchymal stem cells. *Cell Reprogram*. 2019;21(2): 89-98. https://doi.org/10.1089/cell.2018.0040.

39 Mohan KN. DNMT1: catalytic and non-catalytic roles in different biological processes. *Epigenomics*. 2022;14(10):629-643. https://doi.org/10.2217/epi-2022-0035.

40 Syed AA, Reza MI, Garg R, et al. *Cissus quadrangularis* extract attenuates diabetic nephropathy by altering SIRT1/DNMT1 axis. *J Pharm Pharmacol*. 2021;73(11):1442-1450. https://doi.org/10.1093/jpp/rgab078.

41 Zhang L, Zhang QM, Liu SX, et al. DNA methyltransferase 1 may be a therapy target for attenuating diabetic nephropathy and podocyte injury. *Kidney Int*. 2017;92(1):140-153. https://doi.org/10.1016/j.kint.2017.01.010.

42 Jin L, Niu C, Ni YL. Correlation between peripheral blood α1-MG, DNMT1 expression, and the severity of diabetic nephropathy renal pathological damage. *Medicine (Baltimore)*. 2023;102(42):e35409. https://doi.org/10.1097/MD.0000000000035409.

43 Chen GC, Chen HH, Ren SY, et al. Aberrant DNA methylation of mTOR pathway genes promotes inflammatory activation of immune cells in diabetic kidney disease. *Kidney Int*. 2019;96(2):409-420. https://doi.org/10.1016/j.kint.2019.02.020.

44 Zeng S, Wu XY, Chen XY, et al. Hypermethylated in cancer 1 (HIC1) mediates high glucose induced ROS accumulation in renal tubular epithelial cells by epigenetically repressing SIRT1 transcription. *Biochim Biophys Acta Gene Regul Mech*. 2018;1861(10):917-927. https://doi.org/10.1016/j.bbagrm.2018.08.002.

45 Zhao Q, Wang B, Chen S. Application of hederagenin in preparing an antihyperlipidemic drug. China patent CN1385158A. Published December 18, 2002.

46 Su F, Sui X, Xu J, et al. Hederagenin suppresses ovarian cancer via targeting mitochondrial fission through dynamin-related protein 1. *European Journal of Pharmacology*. 2024;963:176188. https://doi.org/10.1016/j.ejphar.2023.176188.

47 Xie ZS, Zhao JP, Wu LM, et al. Hederagenin improves Alzheimer's disease through PPARα/TFEB-mediated autophagy. *Phytomedicine*. 2023;112: 154711. https://doi.org/10.1016/j.phymed.2023.154711.

48 Zeng J, Huang T, Xue M, et al. Current knowledge and development of hederagenin as a promising medicinal agent: a comprehensive review. *RSC Adv*. 2018;8(43):24188-24202. https://doi.org/10.1039/c8ra03666g.